Contents lists available at ScienceDirect

Biomedicine & Pharmacotherapy

Original article

An AKT2-specific nanobody that targets the hydrophobic motif induces cell cycle arrest, autophagy and loss of focal adhesions in MDA-MB-231 cells

Tijs Merckaert [a,b], Olivier Zwaenepoel [a], Kris Gevaert [a,b], Jan Gettemans [a,*]

[a] Department of Biomolecular Medicine, Faculty of Medicine and Health Sciences, Ghent University, Tech Lane Ghent Science Park 75, 9052 Ghent, Belgium
[b] VIB-UGent Center for Medical Biotechnology, Tech Lane Ghent Science Park 75, 9052 Ghent, Belgium

ARTICLE INFO

ABSTRACT

The AKT kinase family is a high-profile target for cancer therapy. Despite their high degree of homology the three AKT isoforms (AKT1, AKT2 and AKT3) are non-redundant and can even have opposing functions. Small-molecule AKT inhibitors affect all three isoforms which severely limits their usefulness as research tool or therapeutic. Using AKT2-specific nanobodies we examined the function of endogenous AKT2 in breast cancer cells. Two AKT2 nanobodies (Nb8 and Nb9) modulate AKT2 and reduce MDA-MB-231 cell viability/proliferation. Nb8 binds the AKT2 hydrophobic motif and reduces IGF-1-induced phosphorylation of this site. This nanobody also affects the phosphorylation and/or expression levels of a wide range of proteins downstream of AKT, resulting in a G0/G1 cell cycle arrest, the induction of autophagy, a reduction in focal adhesion count and loss of stress fibers. While cell cycle progression is likely to be regulated by more than one isoform, our results indicate that both the effects on autophagy and the cytoskeleton are specific to AKT2. By using an isoform-specific nanobody we were able to map a part of the AKT2 pathway. Our results confirm AKT2 and the hydrophobic motif as targets for cancer therapy. Nb8 can be used as a research tool to study AKT2 signalling events and aid in the design of an AKT2-specific inhibitor.

1. Introduction

The phosphoinositide 3-kinase (PI3K)-AKT pathway is the most frequently over-activated pathway in human cancer [1]. Multiple genetic aberrations have been identified in members of this pathway. Examples include the amplification or mutation of receptor tyrosine kinases (RTKs) such as EGFR and HER2, activating mutations in PI3K and PDK1, and loss of PTEN [2,3]. These events result in increased activity of the serine/threonine protein kinase AKT (a.k.a. protein kinase B) [2,4]. AKT is activated by phosphorylation of threonine-309 in the activation loop of the catalytic domain and serine-474 in the C-terminal hydrophobic motif (HM) by PDK1 and mTORC2, respectively. Phosphorylation of both sites enhances AKT stability and is required for maximal catalytic activity [5–7]. Well over a hundred AKT substrates

spanning several functional classes (protein and lipid kinases, regulators of the cell cycle, metabolic enzymes, transcription factors, …) have been identified. Some of these substrates (GSK3α/β, FoxO and mTORC1) are major signalling nodes on their own.

By integrating a wide array of extracellular signals, AKT, as a master kinase regulates cell proliferation, survival, growth, migration and metabolism [5]. This relation of AKT to various hallmarks of cancer, together with the high incidence (>50 %) of AKT hyper-activation in cancer have made this kinase a high-profile target. This has led to the development of several small-molecule inhibitors, some of which have already made it to clinical trials, albeit with limited success [2,8–11]. Both ATP-competitive and allosteric AKT inhibitors have been developed. For ATP-competitive inhibitors, the lack of specificity for AKT is a major issue, which comes as no surprise given the high degree of

similarity of the AKT catalytic domain with such domains from other kinases of the AGC kinase family [12,13]. Allosteric AKT inhibitors, such as MK-2206, which target the PH-domain, show more potential. However, these suffer from the drawback that they affect all AKT isoforms (AKT1/PKBα, AKT2/PKBβ and AKT3/PKBγ), testifying to the difficulty of developing specific AKT inhibitors [14].

The three AKT isoforms are encoded by separate genes and display up to 82 % sequence identity[15]. Despite their highly similar sequences, the isoforms are non-redundant. This was reported in studies using mice with individual knockouts (KO) of AKT isoforms and has been amply confirmed in in vitro studies [3,16–34]. To complicate matters further, their role is also context-dependent and in certain cases opposed to one another. The exact mechanisms that contribute to isoform-specificity have not been fully elucidated, but distinct subcellular localization, differences in relative expression levels and intrinsic kinetic properties, specific (in)activation and mutation of the isoforms are likely to play a role [3,6,26,35–37]. A striking example of isoform-specific functions are the roles of AKT1 and AKT2 in breast cancer, where AKT2 enhances migration and invasion of cancer cells, while AKT1 has the opposite function [21,38–40].

Such observations help to explain the limited success of AKT inhibitors in clinical trials and underline the need for a detailed study of the complex AKT signalling cascades. Mapping each isoform's pathway and developing isoform-specific inhibitors could be the next step in tailoring cancer treatment to be most beneficial for the patient.

In this study we focus on the role of AKT2 in the MDA-MB-231 breast cancer cell model. Instead of relying on genetic approaches to interfere with AKT2, we use nanobodies (Nbs) to target this isoform. Nbs are the antigen-binding fragment of heavy-chain-only antibodies. They consist of a single domain, are small (15 kDa) and highly stable proteins that interact with their antigen with high affinity and specificity [41]. Additionally, Nbs remain functional when expressed in the reducing cytoplasm of mammalian cells, which allows their use for modulating endogenous proteins in a relevant context [42–49]. The AKT2 nanobodies were obtained by immunization of an alpaca with in vitro phosphorylated AKT2 and were previously shown to only interact with the AKT2 isoform [50].

Here, we show that the AKT2 Nbs are high-affinity interactors, which interact only with the AKT2 isoform when stably expressed in MDA-MB-231 cells that express all three AKT isoforms. Nbs 8 and 9 have a cytotoxic/cytostatic effect that is unrelated to apoptosis. We show that Nb8 reduces phosphorylation of the AKT2 HM in IGF-1-stimulated cells and use a (phospho)proteomics approach to map the downstream effects. Our results indicate that AKT2 is a major regulator of the cell cycle, organization of the actin cytoskeleton and autophagy. Nb8 has allowed us to map a part of the AKT2-specific signalling pathway, identified the HM as a therapeutic epitope and further strengthened AKT2 as a *bona fide* target for cancer therapy. This Nb is thus a promising new tool which can be applied, as a complementary approach to genetic approaches, in various contexts to study the function of this AKT isoform and could be used in the rational design of the first AKT2-specific inhibitor by, for instance, co-crystallization and medicinal chemistry [47].

2. Methods

2.1. Antibodies

See Supplementary methods for detailed information on the antibodies used in this study.

2.2. Production and purification of recombinant FL-AKT2

The production of recombinant FL-AKT2 was performed as described previously [50]. Briefly, BL21 *E. coli* were heat-shock transformed and a culture was grown in Terrific Broth (TB, 16.9 mM KH_2PO_4, 71.9 mM $K_2HPO_4.3H_2O$, 2 mM $MgCl_2$, 12 g Tryptone, 24 g yeast extract, 4%

glycerol, 1% glucose pH 7.2) to $OD_{600} \geq 2$, expression was induced with 0.5 mM IPTG and the cultures were incubated ON at 20 °C in a shaking incubator. Cells were lysed using a French press and sonication, debris was pelleted (11,000 x g for 20 min at 4 °C) and the supernatant (SN) was loaded onto a column containing Chitin beads (New England Biolabs). After washing the beads, proteins were eluted by ON incubation with 50 mM DTT and purified by anion exchange chromatography (GE Healthcare). Purity was assessed by SDS-PAGE and Coomassie staining.

2.3. Production of recombinant AKT2 Nbs

WK6 *E. coli* were heat-shock transformed with pMECS-Nb plasmids and grown in TB at 37 °C until an OD_{600} of $0.6-0.8$ was reached. Nb expression was induced by adding 1 mM IPTG and cultures were incubated ON at 28 °C. Nbs in the pMECS vector are expressed with an N-terminal PelB signal sequence, resulting in periplasmatic localization. Cells were pelleted (11,000 x g for 20 min at 4 °C) and Nbs were extracted through osmotic shock using Tris-EDTA-Sucrose (TES, 0.2 M Tris, 0.5 mM EDTA, 0.5 M sucrose, pH 8.00). Protein concentration of the resulting periplasmatic extract was measured using the Bradford assay (Bio-Rad Laboratories).

2.4. Bio-layer interferometry and data processing

All experiments were run on an Octet RED96 system (ForteBio) at 25 °C. Anti-Penta-HIS biosensors (HIS1K, ForteBio) were pre-wet in kinetics buffer (KB, PBS (Gibco, Thermo Fisher) with 0.1 % (w/v) BSA) for at least 10 min. Loading solutions, containing 10 μg/mL protein, were prepared by diluting the Nb-containing periplasmatic extracts in KB. All samples were dispensed into a 96-wellplate (Greiner Bio-One, 655209) at a volume of 200 μl. A single kinetics run entailed the following steps: Biosensor Regeneration (5 s in 0.5 M H_2SO_4 followed by 5 s in KB, for three cycles), Baseline (60 s in KB), Loading (300 s in loading solution), Baseline (60 s in KB), Association (300 s in KB containing purified FL-AKT2) and Dissociation (600 s in KB). Flow rate was set to 1000 for all steps. For Association, four FL-AKT2 concentrations were included (twofold dilutions starting at 25 nM FL-AKT2 for Nbs 5 and 9 or starting at 800 nM for Nb8) and a single reference well without FL-AKT2 for background subtraction. Data was processed (software version 9.0.0.4) using the reference well for subtraction, the baseline was aligned to the y-axis (last 5 s of the Baseline step) and Savitzky-Golay filtering was used to reduce noise. K_D values were generated by fitting (global fit using curves from all AKT2 concentrations) the full association and dissociation steps to a 1:1 kinetic model.

2.5. Cell culture and transduction

For maintenance, MDA-MB-231 (ATCC® HTB-26™) cells were grown at 37 °C in a humidified 10 % CO_2 incubator. The cells were cultured in DMEM supplemented with 10 % foetal bovine serum and 100 IU/mL penicillin and 10 μg/mL streptomycin (medium and supplements from Gibco, Thermo Fisher Scientific). Prior to experiments, all cell lines were tested and found negative for mycoplasma contamination using PlasmoTest™ (InvivoGen). Stable cell lines expressing the AKT2 Nbs and the EGFP Nb were generated using the Lenti-X Tet-On Advanced Inducible Expression System (clontech) as described previously [44].

2.6. Immunofluorescence and microscopy

Coverslips were coated with 50 μg/mL rat tail type I collagen (BD Biosciences) in PBS (with Ca^{2+} and Mg^{2+}) for 1 h at 37 °C. MDA-MB-231 cells were seeded at a density <50 % for Cyclin D1 detection and 60–80 % for all other experiments. 24 h post-seeding, Nb expression was induced with 500 ng/mL Dox (Duchefa Biochemie, D0121) or the cells were treated with 5 μM MK-2206 (Selleckchem). Immunostaining was performed 24 h later. For visualization of autophagic vesicles and

mitochondria, cells were treated with 10 μM Chloroquine for 4 h and incubated with Cyto-ID® green detection reagent (Enzo Life Sciences, ENZ-KIT175) and 0.1 μM MitoTracker™ Orange CMTMRos (Thermo Fisher Scientific, M7510) according to the manufacturer's instructions. Cells were fixed with 3% paraformaldehyde for 25 min, permeabilized with 0.2 % Triton X-100 for 5 min and incubated with 100 mM glycine for 20 min. Each incubation step was followed by at least three washing steps with PBS (with Ca^{2+} and Mg^{2+}). Coverslips were incubated with primary and secondary antibodies (1 h at 37 °C or 30 min at room temperature (RT) for primary Ab and secondary Ab, respectively), nuclei were stained with 0.4 μg/mL DAPI (Sigma Aldrich, D9542) and Acti-stain 670 Phalloidin (Cytoskeleton, PHDN1-A) was used to visualise F-actin. Coverslips were mounted onto microscopy slides using Vecta-shield antifade mounting medium (Vector Laboratories, H-1000) and sealed using nail polish. Images were captured using a Zeiss Axiovert 200 M fluorescence microscope with Apotome module (Zeiss x63 1.4-NA Oil Plan-Apochromat objective, Carl Zeiss) and Axiovision 4.5 software (Zeiss) or an Olympus IX81 Fluoview 1000 confocal laser scanning microscope (Olympus x60 1.36-NA Oil UplanSApo objective, Olympus, Tokyo, Japan) with FluoView FV 1000 software (Olympus). Images were analyzed using ImageJ. For quantifying Cyclin D1 co-localization with DAPI, the Coloc2 plugin was used. A one-way ANOVA with tukey's multiple comparison test (GraphPad Prism v5.00) was used to compare Manders colocalization coefficient with costes thresholding between cell lines. Representative for 85 cells per cell line collected over three repeated experiments. Autophagic vesicles were counted using ImageJ. Focal Adhesion count was determined according to Horzum et al. [51]. A one-way ANOVA with dunnett's multiple comparison test (GraphPad v5.00) was used to determine significant differences in the average number of focal adhesions present in cells.

2.7. Co-immunoprecipitation of AKT2 using intrabodies

Stable cell lines expressing the AKT2 Nbs and EGFP Nb were seeded in T75 cell culture flasks and Nb expression was induced by adding 500 ng/mL Dox. After 24 h, cells were lysed in ice-cold Tris Lysis buffer (20 mM Tris-HCl, 150 mM NaCl, 1% Triton X-100, 1 mM PMSF, 200 μg/mL protease inhibitor cocktail pH 7.5). Cell debris was pelleted and protein concentration determined using the Bradford assay. 1 mg WCL was incubated with 10 μl settled anti-V5-agarose beads (A7345, Sigma Aldrich) for 1 h at 4 °C with end-over-end rotation. The beads were washed three times and proteins were eluted in Laemmli SDS sample buffer (5% SDS, 20 % glycerol, 0,2% bromophenol blue, 5% β-mercap-toethanol, 65 mM Tris-HCl pH 6.8) by heating the beads to 95 °C for 5 min. Eluates were analysed by SDS-PAGE and Western blotting. D6G4 was used to detect AKT2 and Nbs were detected using an anti-V5 Ab (Invitrogen, 1296025).

2.8. XTT assay

Stable MDA-MB-231 cell lines expressing the AKT2 Nbs or EGFP Nb were detached using Trypsin-EDTA (Gibco, Thermo Fisher Scientific) and re-seeded at 6,000 cells per well in 96-wellplates (Greiner Bio-One, 655160). A separate plate was used for each time point (24 h, 48 h and 72 h). 500 ng/mL Dox was added to induce Nb expression. An internal control condition without Dox and background correction wells containing only medium (no cells) were also included. After incubation (24−72 h) 50 μl of activated XTT solution (XTT cell proliferation kit II, Roche) was added to all wells and the OD was measured at 475 nm and 660 nm, immediately (background), 4 h and 6 h after adding the solution. Specific absorbance was obtained by subtracting the values from background wells and non-specific readings (OD at 660 nm). Values were normalized for the internal control and the EGFP Nb-expressing cells. Data was gathered from three independent experiments. A one-way ANOVA with tukey's multiple comparison test (GraphPad Prism v 5.00) was used to compare all time points within a single cell line or a

single time point between all cell lines.

2.9. Caspase-3 detection

Stable MDA-MB-231 cell lines expressing AKT2 Nbs or the EGFP Nb were seeded in 6-wellplates at a density of 75,000 cell per well and Nb expression was induced by adding 500 ng/mL Dox. Cells were lysed with ice cold Tris Lysis buffer, immediately, 24 h, 48 h and 72 h after adding Dox. Staurosporine-treated (10 μM, 24 h) cells were included as positive control. Protein concentration in the WCL was determined by Bradford assay and a 10 μg sample was analysed by SDS-PAGE and Western blotting. The Caspase-3 Ab used (Cell Signaling Technology, 9662) detected both full-length Caspase-3 and the 17/19 kDa fragments. Vinculin (hVIN-1, Sigma Aldrich) was used as loading control and Nbs were detected through their V5-tag.

2.10. AKT2 hydrophobic motif phosphorylation

MDA-MB-231 cell stably expressing Nb8 were seeded in a 6-wellplate. Cells were serum starved for 48 h and Nb expression was induced with 500 ng/mL Dox for 24 h. A control condition of serum starved cells without Dox was included. Cells were stimulated with 5 ng/mL IGF-1 for 1 min, 5 min, 15 min or 30 min and lysed using ice cold RIPA lysis buffer (25 mM Tris-HCl, 150 mM NaCl, 1% NP-40, 1% sodium deoxycholate, 0.1 % SDS, 1 mM PMSF, 200 μg/mL protease inhibitor cocktail mix, pH 7.6) with phosphatase inhibitors (PhosSTOP™, Roche, 1 tablet/10 ml buffer). A 10 μg sample was analysed by SDS-PAGE and western blotting. AKT2 and p-AKT2 S474 were detected using D6G4 and D3H2, respectively. Vinculin was used as loading control and Nb8 was detected using an anti-V5-tag Ab. Signal intensity was quantified using ImageJ. A one-way ANOVA (GraphPad Prism v5.00) was used to compare signal intensity in Nb8-expressing cells with un-induced counterparts.

2.11. (Phospho)proteomics analysis

2.11.1. Sample preperation

Stable MDA-MB-231 cells expressing Nb8 or the EGFP Nb were serum-starved for 48 h and treated with Dox (500 ng/mL) for 24 h prior to IGF-treatment (5 ng/mL, 5 min) and lysis. Cells were scraped and lysed in a urea lysis buffer containing 9 M urea, 20 mM HEPES pH 8.0 and PhosSTOP™ phosphatase inhibitor cocktail (Roche, 1 tablet/10 ml buffer). The samples were sonicated with 3 pulses of 15 s at an amplitude of 20 % using a 3 mm probe, with incubation on ice for 1 min between pulses. After centrifugation for 15 min at 20,000 x g at RT to remove insoluble components, proteins were reduced by addition of 5 mM DTT and incubation for 30 min at 55 °C and then alkylated by addition of 10 mM iodoacetamide and incubation for 15 min at RT in the dark. The protein concentration was measured using a Bradford assay and, from each sample, 4 mg protein was used to continue the protocol. Samples were further diluted with 20 mM HEPES pH 8.0 to a final urea concentration of 4 M and proteins were digested with 40 μg LysC (Wako) (1/100, w/w) for 4 h at 37 °C. Samples were diluted to 2 M urea and digested with 40 μg trypsin (Promega) (1/100, w/w) overnight at 37 °C. The resulting peptide mixture was acidified by addition of 1% tri-fluoroacetic acid (TFA) and after 15 min incubation on ice, samples were centrifuged for 15 min at 1,780 x *g* at room temperature to remove insoluble components. Next, peptides were purified on SampliQ SPE C18 cartridges (500 mg, Agilent). Columns were first washed with 5 ml 100 % acetonitrile (ACN) and pre-equilibrated with 15 ml of solvent A (0.1 % TFA in water/ACN (98:2, v/v)) before samples were loaded on the column. After peptide binding, the column was washed again with 5 ml of solvent A and peptides were eluted twice with 700 μl elution buffer (0.1 % TFA in water/ACN (20:80, v/v)). The eluted peptides were divided in two parts: 100 μl was dried completely in a speedvac vacuum concentrator for shotgun analysis, while the remainder was used for phosphopeptide enrichment. Phosphopeptides were enriched with

MagReSyn® Ti-IMAC beads according to the manufacturer's instructions with slight modifications. Briefly, 100 µl MagReSyn® Ti-IMAC beads (per sample) were washed twice with 70 % EtOH, once with 1% NH_4OH and three times with a mixture of water/ACN/TFA (14:80:6, v/v/v). Next, the digested sample was incubated with the washed beads for 30 min at room temperature, the beads were washed once with a mixture of water/ACN/TFA (14:80:6, v/v/v) and three times with a mixture of water/ACN/TFA (19:80:1, v/v/v). Phosphopeptides were eluted from the beads by adding 80 µl 1% NH_4OH three times. 60 µl 10 % formic acid (FA) was added to the combined eluate and the samples were dried completely in a speedvac vacuum concentrator.

2.11.2. LC–MS/MS analysis

LC–MS/MS analysis was performed at the VIB Proteomics Core. Purified peptides for shotgun analysis were re-dissolved in 20 µl solvent A and 2 µl of each sample was injected for LC–MS/MS analysis on an Ultimate 3000 RSLCnano system (Thermo) in line connected to a Q Exactive mass spectrometer (Thermo). Trapping was performed at 10 µl/min for 4 min in loading solvent A on a 10 mm µPAC™ trapping column (PharmaFluidics) with C18-endcapped stationary phase and the samples were loaded on a 50 cm long micro pillar array column (PharmaFluidics) with C18-endcapped functionality mounted in the Ultimate 3000's column oven set at 35 °C. For proper ionization, a fused silica PicoTip emitter (10 µm inner diameter, New Objective) was connected to the µPAC™ outlet union and a grounded connection was provided to this union. Peptides were eluted by a non-linear increase from 1 to 50 % MS solvent B (0.1 % FA in water/ACN (2:8, v/v)) over 159 min, first at a flow rate of 750 nl/min, then at 300 nl/min, followed by a 5-minutes wash reaching 95 % MS solvent B and re-equilibration with MS solvent A (0.1 % FA in water). The mass spectrometer was operated in data-dependent, positive ionization mode, automatically switching between MS and MS/MS acquisition for the 5 most abundant peaks in a given MS spectrum. The source voltage was 2.9 kV, and the capillary temperature was 275 °C. One MS1 scan (m/z $400 − 2,000$, AGC target 3×10^6 ions, maximum ion injection time 80 ms), acquired at a resolution of 70,000 (at 200 m/z), was followed by up to 5 tandem MS scans (resolution 17,500 at 200 m/z) of the most intense ions fulfilling predefined selection criteria (AGC target 5×10^4 ions, maximum ion injection time 80 ms, isolation window 2 Da, fixed first mass 140 m/z, spectrum data type: centroid, intensity threshold 1.3xE^4, exclusion of unassigned, 1, 5–8, >8 positively charged precursors, peptide match preferred, exclude isotopes on, dynamic exclusion time 12 s). The HCD collision energy was set to 25 % Normalized Collision Energy and the polydimethylcyclosiloxane background ion at 445.120025 Da was used for internal calibration (lock mass).

Peptides resulting from phosphopeptide enrichment were re-dissolved in 20 µl solvent A and 10 µl was injected for LC–MS/MS analysis on an Ultimate 3000 RSLCnano system in-line connected to a Q Exactive HF mass spectrometer equipped with a Nanospray Flex Ion source (Thermo). Trapping was performed at 10 µl/min for 4 min in solvent A on a 20 mm trapping column (made in-house, 100 µm internal diameter (I.D.), 5 µm beads, C18 Reprosil-HD, Dr. Maisch, Germany) and the samples were loaded on a 50 cm long micro pillar array column (PharmaFluidics) with C18-endcapped functionality mounted in the Ultimate 3000's column oven set at 35 °C. For proper ionization, a fused silica PicoTip emitter (10 µm inner diameter) (New Objective) was connected to the µPAC™ outlet union and a grounded connection was provided to this union. Peptides were eluted by a non-linear increase from 1 to 50 % MS solvent B (0.1 % FA in water/ACN (2:8, v/v)) over 159 min, first at a flow rate of 750 nl/min, then at 300 nl/min, followed by a 5-minutes wash reaching 95 % MS solvent B and re-equilibration with MS solvent A (0.1 % FA in water). The mass spectrometer was operated in data-dependent, positive ionization mode, automatically switching between MS and MS/MS acquisition for the 5 most abundant peaks in a given MS spectrum. The source voltage was 2.6 kV, and the capillary temperature was 275 °C. One MS1 scan (m/z $400 − 2,000$, AGC target 3×10^6 ions, maximum ion injection time 80 ms), acquired at a resolution of 70,000 (at 200 m/z), was followed by up to 5 tandem MS scans (resolution 17,500 at 200 m/z) of the most intense ions fulfilling predefined selection criteria (AGC target 5×10^4 ions, maximum ion injection time 80 ms, isolation window 2 Da, fixed first mass 140 m/z, spectrum data type: centroid, intensity threshold 1.3xE^4, exclusion of unassigned, 1, 5–8, >8 positively charged precursors, peptide match preferred, exclude isotopes on, dynamic exclusion time 12 s). The HCD collision energy was set to 25 % Normalized Collision Energy and the polydimethylcyclosiloxane background ion at 445.120025 Da was used for internal calibration (lock mass). QCloud was used to control instrument longitudinal performance during the project [52].

2.11.3. Data processing

Data processing was performed at the VIB Proteomics Core. Data analysis of the shotgun and phosphoproteomics data was performed with MaxQuant (version 1.6.10.43) using the Andromeda search engine with default search settings including a false discovery rate set at 1% on PSM, peptide and protein level. Spectra were searched against the human proteins in the UniProt Reference Proteome database (database release version of June 2019 containing 20,960 human protein sequences, (http://www.uniprot.org) supplemented with the sequences of AKT2 Nb8 and the EGFP Nb. The mass tolerance for precursor and fragment ions was set to 4.5 and 20 ppm, respectively, during the main search. Enzyme specificity was set as C-terminal to arginine and lysine, also allowing cleavage at proline bonds with a maximum of two missed cleavages. Variable modifications were set to oxidation of methionine residues, acetylation of protein N-termini and phosphorylation of serine, threonine or tyrosine residues, while carbamidomethylation of cysteine residues was set as fixed modification. Matching between runs was enabled with a matching time window of 0.7 min and an alignment time window of 20 min. Only proteins with at least one unique or razor peptide were retained leading to the identification of 3,805 proteins and 9,999 phosphorylated sites. Proteins were quantified by the MaxLFQ algorithm integrated in the MaxQuant software. A minimum ratio count of two unique or razor peptides was required for quantification.

2.11.4. Data analysis

Further data analysis of the shotgun results was performed with the Perseus software (version 1.6.2.1) after loading the proteingroups file from MaxQuant. Reverse database hits, potential contaminants and proteins that were only identified by site were removed, LFQ intensities were log2 transformed and replicate samples were grouped. Proteins with less than three valid values in at least one group were removed and missing values were imputed from a normal distribution (width 0.3 and down shift 1.8) around the detection limit leading to a list of 2,509 quantified proteins that was used for further data analysis. Then, a t-test was performed (FDR = 0.05 and s0 = 0) and significant hits were filtered for Log_2LFQ(Nb8/EGFP Nb) difference of <-1 or >1 to compare differences in protein levels between Nb8- and EGFP Nb-expressing cells. A volcano plot was generated. 37 proteins were found to be significantly regulated.

For the analysis of the phosphoproteome data, the phospho(STY) sites file was loaded in the Perseus software (version 1.6.2.1). Reverse hits and potential contaminants were removed, the site table was expanded and the intensity values were log2 transformed. Replicate samples were grouped, phosphosites with less than three valid values in at least one group were removed and missing values were imputed from a normal distribution (width 0.3 and down shift 1.8) around the detection limit leading to a list of 7,677 quantified phosphopeptides that was used for further data analysis. Then, a t-test was performed (FDR = 0.05 and s0 = 0) and significant hits were filtered localization probability ≥0.75 and for Log_2LFQ(Nb8/EGFP Nb) difference of <-1 or >1 to compare Nb8- and EGFP Nb-expressing cells. A volcano plot was generated. 189 phosphopeptides were significantly regulated.

The Panther classification system was used to determine statistical overrepresentation of GO-terms in the list of significantly regulated

proteins. The whole *Homo sapiens* gene set was used as reference list, a Fisher's exact test with Bonferroni correction for multiple testing was used to determine significantly enriched (p < 0.05) terms.

The mass spectrometry proteomics data have been deposited to the ProteomeXchange Consortium via the PRIDE partner repository with the dataset identifier PDX020637 (login username: reviewer19716@ebi.ac.uk and password: iJKACkge).

2.12. Detection of cyclin D1 expression levels

MDA-MB-231 cell lines (parental, EGFP Nb, Nb5, Nb8 and Nb9) were seeded in 6-wellplates at 80,000 cells / well. Nb expression was induced by Dox (500 ng/mL). A control condition of untreated cells and cells treated with 5 µM Mk-2206 were also included. After 24 h incubation, cells were lysed using RIPA lysis buffer and 10 µg WCL was analysed through SDS-PAGE and western blotting. P-AKT2 S474 was detected using D3H2, Cyclin D1 using Ab16663, Vinculin by hVIN-1 and Nbs through their V5-tag. Vinculin was used as loading control. Signal intensity was quantified using ImageJ and a Wilcoxon signed rank test (GraphPad Prism v5.00) was used to compare treated cells with control conditions.

2.13. Cell cycle analysis

180,000 cells were seeded in 25 cm^2 culture flasks and treated with Dox (500 ng/mL) for 24 h. Cells were detached, fixed with ice cold 70 % ethanol for 30 min and permeabilized with 0.2 % Tween-20 and 0.2 % saponin in PBS. After blocking in 5 % (w/v) BSA and 0.2 % Tween-20 in PBS cells were incubated for 1 h at RT with 1 µg/mL anti-V5-AF645 (Thermo Fisher Scientific, 451098). Cells were washed twice with PBS between incubation steps. Finally, the cells were incubated with 100 µg/mL RNase A (Roche) for 5 min at RT and subsequently with 50 µg/mL Propidium Iodide (Sigma Aldrich, P4170). Samples were run on an Attune NxT Flow Cytometer (Invitrogen). The obtained data was analysed with FlowJo™ (v10). Samples were gated to exclude cellular debris and doublets. A one-way ANOVA with Tukey's multiple comparison test (GrahPad Prism v5.00) was used to determine significant changes in the proportion of cells in each cell cycle phase.

2.14. Detection of LC3B-II

MDA-MB-231 cells (parental, EGFP Nb, Nb5, Nb8 or Nb9) were seeded in 6-wellplates at 100,000 cells/well. After ON incubation cells were treated (5 µM Mk-2206 for the parental cells and 500 ng/mL Dox for stable cell lines) and incubated for 24 h. untreated cells were included as a control, as well as cells which were, in addition to Mk-2206 or Dox, also treated with 100 mM NH$_4$Cl for 4 h. Cells were lysed using ice cold RIPA lysis buffer and a 25 µg sample was analysed by SDS-page and western blotting. The LC3B Ab (Cell Signaling Technology, 2775) detected both LC3B-I and LC3B-II. Actin (Abcam, Ab8229) was used as loading control, Nbs were detected using their V5-tag. Signal was quantified using ImageJ and a Wilcoxon signed rank test (GraphPad Prism v5.00) was used to detect significant differences between treated cells and control.

2.15. Quantification of CD29 levels

MDA-MB-231 cells expressing Nb8 or the EGFP Nb were seeded in 6-wellplates. Nb expression was induced by Dox (500 ng/mL) and cells were lysed immediately, after 24 h and 48 h using ice cold RIPA lysis buffer. A 10 µg sample was analysed by SDS-page and western blotting. CD29 was detected using P5D2 (Abcam, 24693) and Nbs using an anti-V5 Ab. GAPDH (Abcam, Ab8245) was used as loading control. Signal intensity was quantified using ImageJ and a one-way ANOVA with dunnett's multiple comparison test (GraphPad v5.00) to analyse differences between time points.

3. Results

3.1. The AKT2 Nbs are high-affinity interactors

To further characterize the obtained nanobodies we determined detailed binding characteristics with AKT2 (stoichiometry, k_{on} & k_{off}) through Bio-layer Interferometry (Fig. 1A-C). The obtained binding
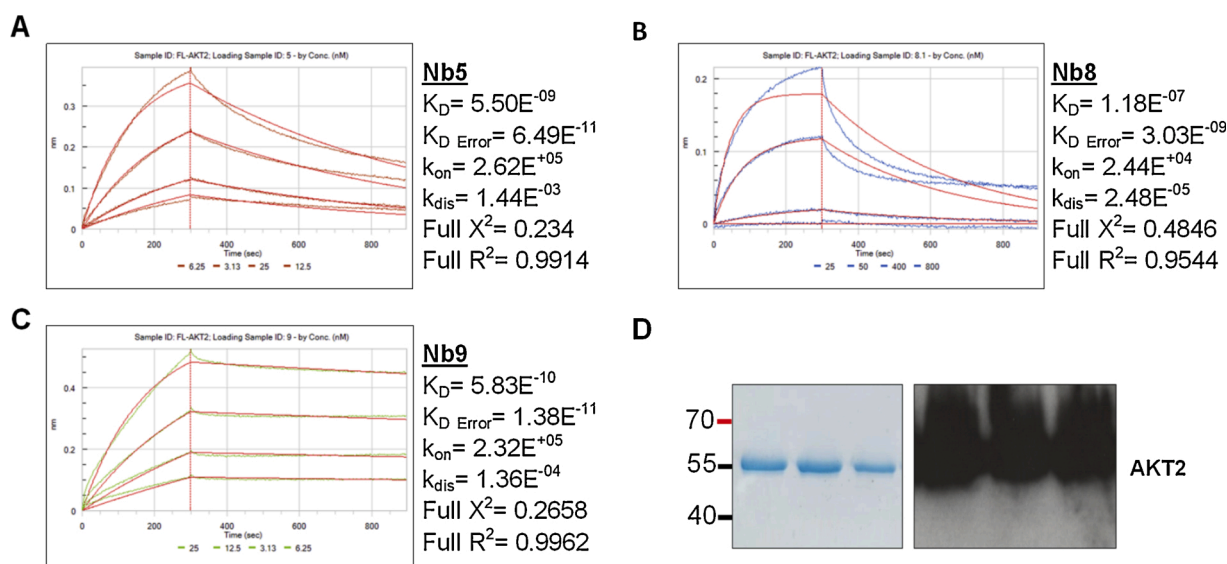

Fig. 1. Bio-layer interferometry for AKT2 Nbs.
A-C: association and dissociation curves for the interaction of AKT2 Nbs 5, 8 and 9 with FL-AKT2. Nbs with a C-terminal HA-His$_6$-tag, obtained from an *E. coli* periplasmatic extract, were loaded onto biosensors coated with an anti-penta-His Ab. After measuring the background in the buffer, the tips were dipped into buffer solution containing AKT2 at various concentrations (association) and subsequently into a well containing only buffer for dissociation. The binding and release of AKT2 produced a shift in the interference pattern of reflected light, which was measured in real-time, resulting in the shown binding curves. **D:** SDS-PAGE and Western blot of human FL-AKT2 (UniProt P31751) which was produced as an intein fusion protein in BL21 *E. coli* and purified using the IMPACT™ system followed by anion-exchange chromatography. Column fractions 28–30 are shown. Purity was assessed by SDS-PAGE and Western blotting using an AKT2 specific Ab. The uncropped gel and blot are available in Supplementary Fig. S1.

curves, for all Nbs, were fit using a 1:1 binding kinetic model. X^2 and R^2 values were < 3 and > 0.95, respectively, which indicated that this was a good fit. All AKT2 Nbs interacted with recombinantly produced AKT2 with (sub)nanomolar affinity: Nb5 $K_D = 5.5$ nM $\pm$ 64.9 pM, Nb8 $K_D = 118$ nM $\pm$ 3.03 nM and Nb9 $K_D = 583$ pM $\pm$ 13.8 pM.

3.2. Modulation of AKT2 in cancer cells

3.2.1. Generation of stable cell lines expressing the AKT2 Nbs as intrabodies

Previous experiments indicated that AKT2 Nb5, 8 and 9 only interact with the AKT2 isoform [50]. Using these Nbs as intrabodies (Nbs expressed intracellularly) would allow us to study the function of AKT2 without perturbing the other two isoforms. The AKT2 Nbs and EGFP Nb were subcloned into the lentiviral, tetracycin-inducible pLVX-Tight-Puro expression vector and transduced into MDA-MB-231 human breast cancer cells. Stable MDA-MB-231 cell lines with doxycycline (Dox)-inducible expression of the AKT2 Nbs or the EGFP Nb were generated (Fig. 2A). All nanobodies were successfully expressed in the stable cell lines. Co-immunoprecipitation (Co-IP) experiments to assess the intrabody-AKT2 interaction showed that all AKT2 Nbs were able to pull-down AKT2 (Fig. 2B). The EGFP Nb-expressing cell line was used as control. Using the same procedure, no AKT1 or AKT3 could be detected in a Co-IP experiment (Supplementary Fig. S2).

3.2.2. Nb8 and Nb9 negatively regulate MDA-MB-231 cell viability or proliferation

Several cellular processes regulated by AKT2 directly affect cell viability or metabolism. XTT and clonogenic assays were performed to determine whether the Nbs have a cytostatic/cytotoxic effect on MDA-MB-231 cells (Fig. 3A and Supplementary Fig. S4). Both the parental cell line and the stable cell line expressing the EGFP Nb were used as controls. The effect of Nb expression was measured for up to 72 h at intervals of 24 h. A 2-way ANOVA showed that there was significant interaction ($F(8,44) = 5.78$, $p \leq 0.0001$) between Nb and expression time (a time-dependent effect of Nb expression on OD_{475} of the formazan dye). Simple effects analysis by one-way ANOVA showed, that for all measured time points (24, 48 and 72 h), cells expressing either Nb8 or Nb9 had significantly ($p < 0.05$) lower mean OD_{475} when compared to the parental cell line and EGFP Nb- or Nb5-expressing cell lines. Cells expressing Nb5 did not exhibit a significant ($p > 0.05$) shift in mean OD_{475} compared to the controls indicating that, at any of the measured time points, Nb5 did not affect viability or cell division. Both Nb8 and Nb9 had a time-dependent effect on OD_{475} with significantly lower values after 48 h compared to 24 h. However, the effect of these Nbs appeared to reach a maximum after 48 h. Additionally, Nb8 and Nb9 elicited a comparable effect on the cells as their mean OD_{475} was not significantly different at any time point. These results indicate that the interaction of Nb8 or Nb9 with AKT2 negatively affects its function,
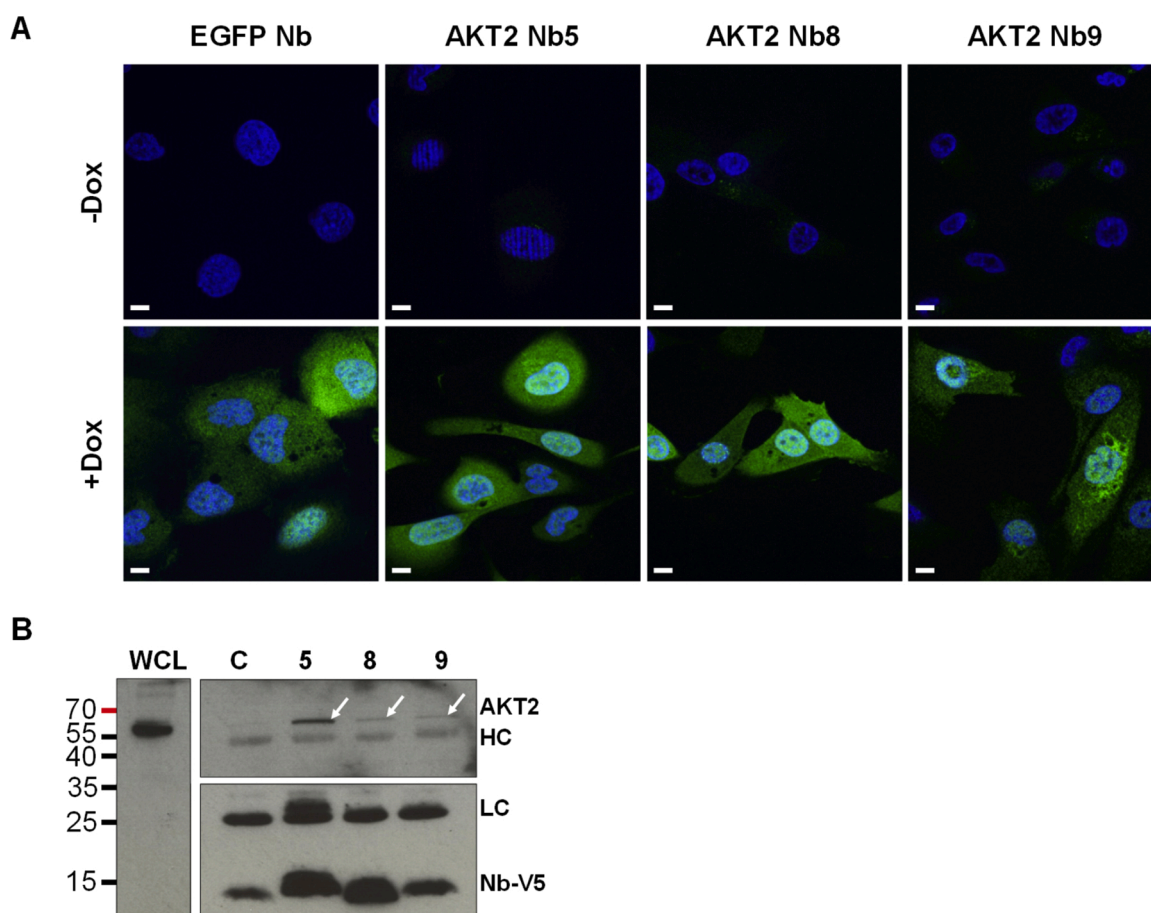

Fig. 2. AKT2 Nbs as intrabodies in MDA-MB-231 cells.
A: Stable and inducible expression of the EGFP Nb and AKT2 Nbs in MDA-MB-231 cells. Representative epifluorescence images of stable MDA-MB-231 cells with Dox-inducible Nb expression. Nb expression was induced with 500 ng/mL Dox (+**Dox**), uninduced cells (-**Dox**) were included to assess leakage expression. Merged images are shown, nuclei were visualized by DAPI (**blue**) and Nbs with an anti-V5 Ab (**green**). Scale bar, 10 μm. **B:** Co-IP of endogenous AKT2 from stable MDA-MB-231 cells with V5-tagged intrabodies using anti-V5 agarose. Nb expression was induced with 500 ng/mL Dox. **WCL**= whole cell lysate, **C**= control using the EGFP Nb-expressing stable cell line. **HC**= Heavy-Chain, **LC**= Light-Chain. All Nbs were expressed in the stable cell lines and only the AKT2 Nbs pulled-down AKT2. AKT2 was detected using an isoform-specific Ab, Nbs were detected through their V5-tag. Co-IPs for AKT1, AKT3 and uncropped blots are available in Supplementary Fig. S3.
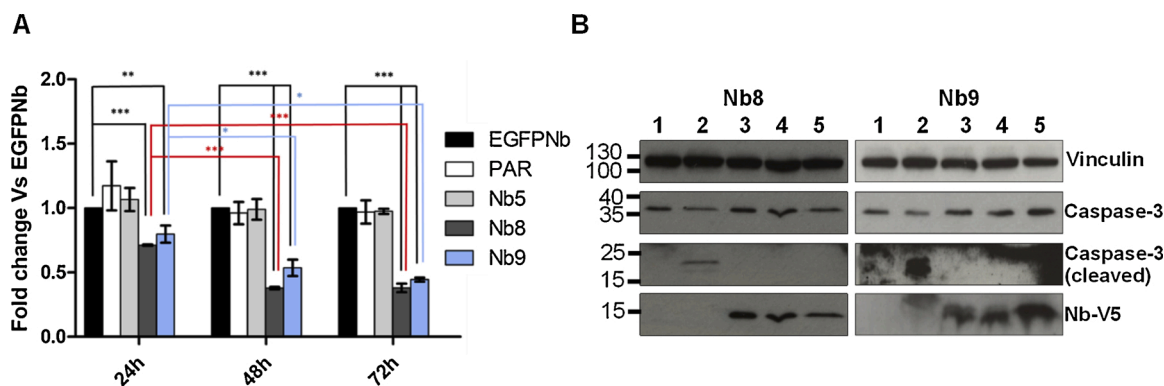
Fig. 3. Cytotoxic and cytostatic effect of AKT2 intrabodies on MDA-MB-231 cells.
A: XTT-assay of the Parental (**PAR**) and stable MDA-MB-231 cell lines expressing the EGFP Nb or AKT2 Nb5, 8 and 9. Both the Parental and EGFP Nb-expressing cell lines were used as negative control. Values shown are the mean and SD of OD_{475} values normalized for the EGFP Nb for three repeated experiments. A one-way ANOVA with Tukey's multiple comparison test was used to compare mean OD_{475} values. * $p < 0.05$, ** $p < 0.01$, ***$p < .001$. Full statistical analysis can be found in Supplementary Table S1. **B:** Western blot detection of caspase-3 processing in AKT2 Nb8- or Nb9-expressing MDA-MB-231 cells. **1**= untreated, **2**= Staurosporine (10 μM), **3** = 24 h 500 ng/mL Dox, **4**= 48 h 500 ng/mL Dox, **5**= 72 h 500 ng/mL Dox. The 17 and 19 kDa fragments of caspase-3 could not be detected in cells expressing Nb8 or Nb9, indicating that the observed reduction in cell count was not a consequence of apoptosis. Vinculin was used as loading control. Uncropped blots are available as Supplementary Fig. S5.

possibly through different mechanisms as they bind separate epitopes [50]. Although it has been shown that pan-AKT inhibition induces apoptosis, our results indicated that this was not the case for Nb8 or Nb9 (Fig. 3B) [53]. No reduction in full length caspase-3 nor the presence of cleaved Caspase-3 could be detected in cells expressing Nb8 or Nb9 for up to 72 h whereas staurosporine, the positive control, induced both. Considering that caspase-3 is activated at the end of both intrinsic and extrinsic apoptotic pathways, these results strongly argue against the involvement of this cell death mechanism in the effects observed in the XTT-assay. Additionally, we did not observe the typical changes in cell shape nor detachment of cells from substrate, signs of apoptosis, in Nb-expressing cells. This was however the case in staurosporine-treated cells.

3.2.3. Nb8 affects AKT2 HM phosphorylation in IGF-1 stimulated cells

Epitope mapping experiments showed that Nb8 interacts with the AKT2 HM and Nb9 with the pleckstrin homology (PH) domain [50]. Both Nbs can potentially interfere with AKT2 activation: Nb8 by shielding the modification site in the HM and Nb9 by interfering with the PH-phosphatidylinositol 3,4,5-trisphosphate $(PtdIns(3,4,5)P_3)$ interaction [6,7,50]. The effect of the AKT2 Nbs on phosphorylation of the AKT2 HM was determined through Western blotting (Fig. 4A). In cells expressing Nb8 we observed a clear and significant reduction (one-way ANOVA, **p < 0.0001**) in pAKT2 S474 levels after 1, 5 and 30

min IGF-1 stimulation but not after 15 min IGF-1 stimulation (Fig. 4B). Such an effect was not observed in Nb5-, Nb9- or EGFP Nb-expressing cells. Total AKT2 levels were unchanged at any of the measured time points (one-way ANOVA, $p < 0.05$).

3.2.4. Nb8 expression resulted in significant changes in the (phospho) proteome

The AKT kinases are part of a large signalling cascade involving downstream kinases and transcription factors. AKT2's phosphorylation status determines its catalytic activity and, possibly, which substrates can be phosphorylated by the kinase [54,55]. To obtain a comprehensive view of Nb8's effects on AKT2 signalling, the proteome and phosphoproteome of MDA-MB-231 cells expressing Nb8 or the EGFP Nb were compared. Using a label-free approach we were able to reliably quantify 2,509 proteins and 7,677 phosphosites on 1,998 proteins. A student's *t*-test and filtering by difference in intensity resulted in the identification of 151 down- and 38 up-regulated phosphosites (Fig. 5A). As changes in regulation of a protein modification (phosphosite) can reflect changes in regulation of the whole protein, protein expression levels in the same samples were quantified (shotgun proteome (SG) analysis) prior to phosphoprotein enrichment. Fold change values of phosphosites, for which the whole protein could be quantified, were normalized. This was possible for 74 phosphosites (39 % of all identified phosphosites). The SG proteome analysis indentified 37 differentially regulated proteins (20
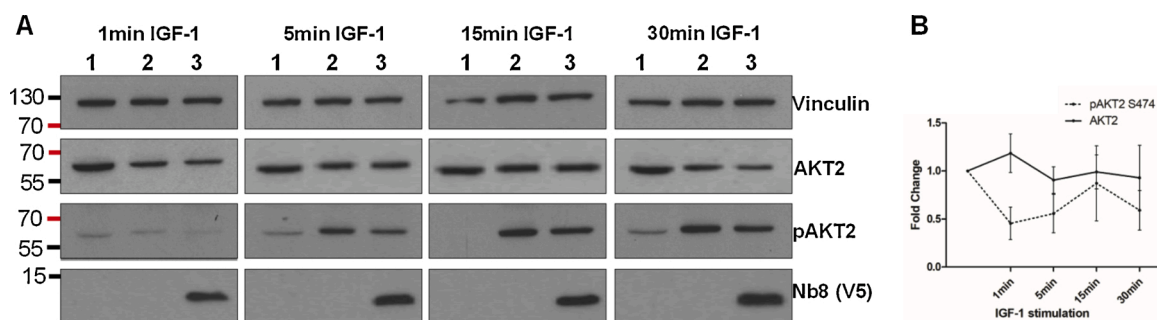

Fig. 4. Nb8 expression attenuates IGF-1 response in MDA-MB-231 cells.
A: Western blot detection of HM-phosphorylated AKT2 (pAKT2 S474). **1**= cells grown in standard growth medium, **2**= 48 h serum starved and IGF-1 (5 ng/mL) stimulated cells without Nb8 expression and **3**= 48 h serum starved and IGF-1 (5 ng/mL) stimulated cells with Nb8 expression (500 ng/mL Dox). Vinculin was used as loading control and Nb8 was detected through its V5-tag. AKT2 and pAKT2 S474 were detected using isoform-specific Abs. Uncropped blots are available in Supplementary Fig. S6. **B:** ImageJ quantification of AKT2 and pAKT2 S474 levels. Values were normalized for vinculin. The fold change of AKT2 and pAKT2 S474 levels between Nb8-expressing cells and uninduced cells was calculated. A one-way ANOVA indicated there was a significant reduction in pAKT2 S474 levels for Nb8-expressing cells after 1, 5 and 30 min IGF-1 stimulation. Total AKT2 levels did not significantly differ for any time point.
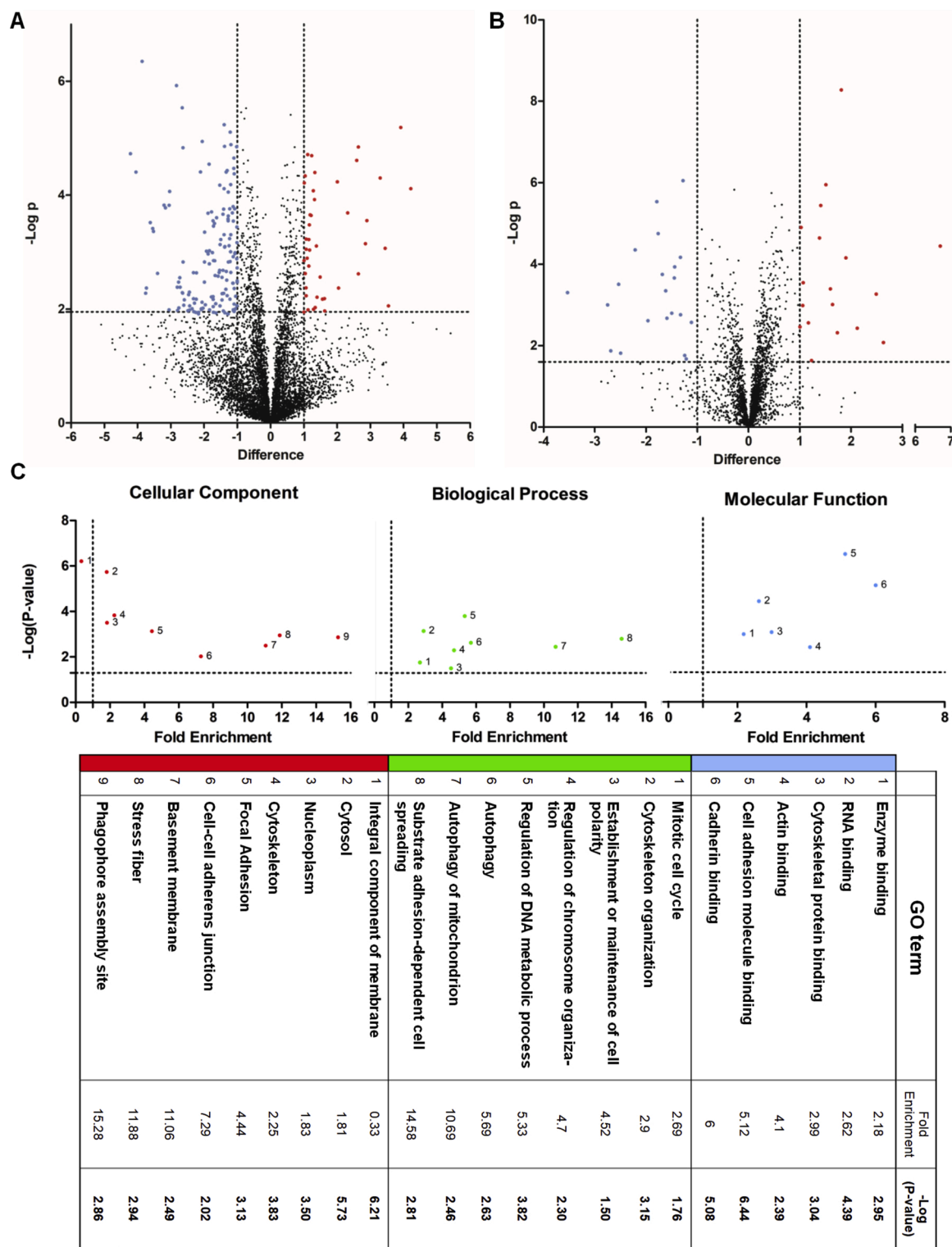
Fig. 5. Differential (phospho)proteome analysis of Nb8- vs EGFP Nb-expressing cells.
Relative phosphopeptide (**A**) or protein (**B**) intensities (Log$_2$LFQ(Nb8/EGFP Nb)) are plotted versus statistical significance (-Log$_{10}$(P value, two-sided student's t-test)). Quantified peptides were filtered by significance (permutation-based false discovery rate calculation, FDR = 0.05 S0 = 0) and a difference ≥1 or ≤-1. Hits which were up-regulated in Nb8-expressing cells are indicated in red, down-regulated hits in blue. **C:** A selection of enriched GO terms with fold change and p-value are plotted, divided into three categories: 'cellular component', 'biological process' and 'molecular function'.

down- and 17 up-regulated proteins) in Nb8-expressing cells (Fig. 5B). The full list of differentially regulated phosphosites and proteins can be found in Supplementary Proteomics Data. Both PCA analysis of all quantified phosphosites or proteins and hierarchical clustering of differentially regulated proteins/phosphosites clearly grouped the

replicate samples by 'treatment' i.e. Nb8 or EGFP Nb expression (Supplementary Fig. S7).

AKT2 protein expression was not differentially regulated between EGFP Nb- and Nb8-expressing cells, but no phosphorylated AKT2 peptides were identified. For both AKT1 and AKT3, phosphopeptides were
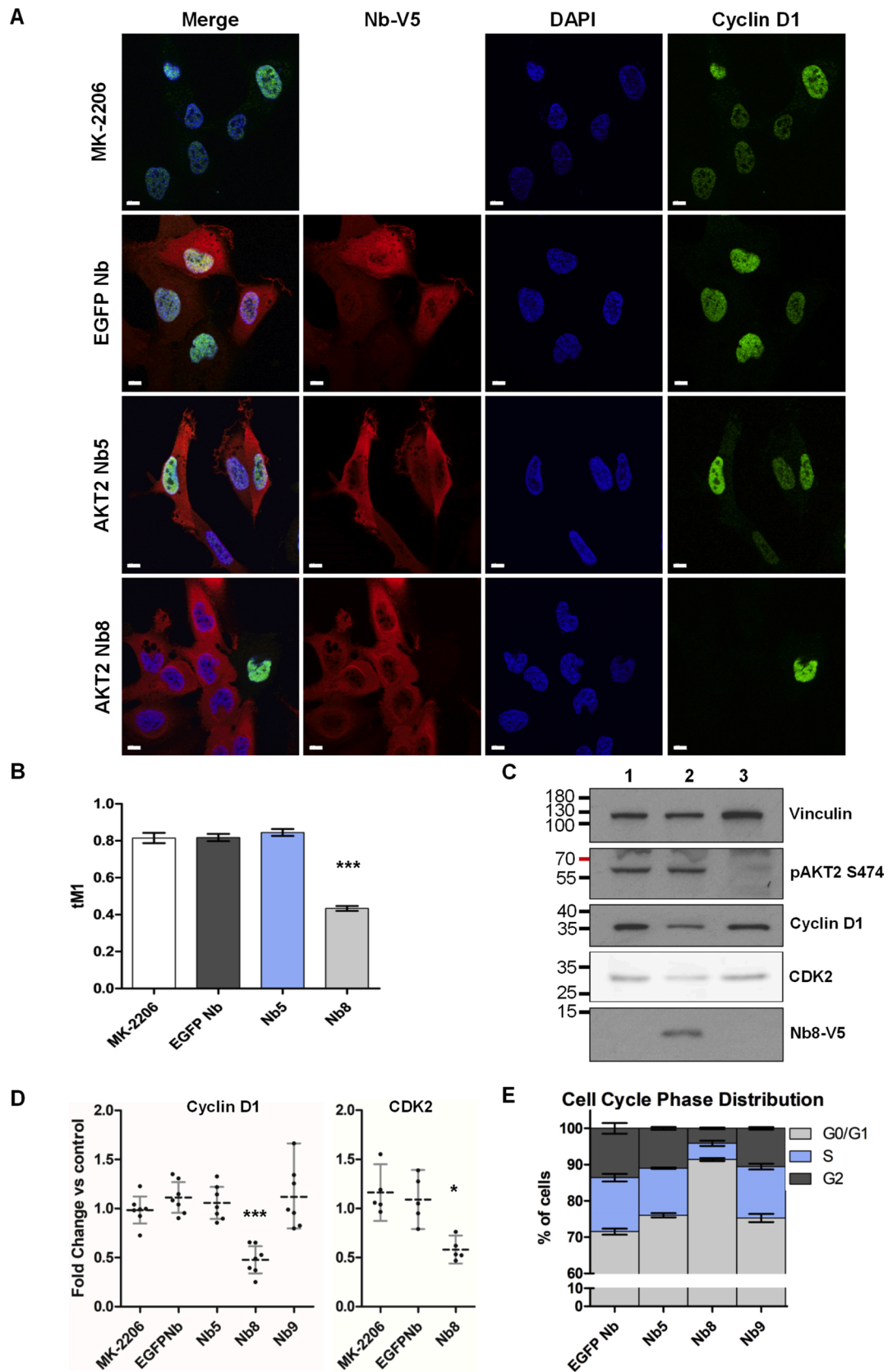
(caption on next page)

Fig. 6. Nb8 expression affected cell cycle progression through Cyclin D1 regulation.
A: Representative epifluorescence images of MDA-MB-231 cells treated with 5 μM MK-2206 or stably expressing AKT2 Nb5, Nb8 or the EGFP Nb (500 ng/mL Dox). The Nbs were distributed equally throughout the cells (**red**). In cells treated with MK-2206 or expressing Nb5 or the EGFP Nb, the signal for Cyclin D1 (**green**) coincided with the signal for DAPI (**blue**), indicating a nuclear enrichment of Cyclin D1. In Nb8-expressing cells this nuclear staining pattern was lost. Scale bar, 10 μm. **B:** Plotted mean and 95 % CI of Manders' Colocalization Coefficient after Costes thresholding (**tM1**) for DAPI and Cyclin D1 for at least 85 cells. A one-way ANOVA with Tukey's multiple comparison test indicated tM1 for Nb8-expressing cells was significantly (**p < 0.0001**) lower compared to tM1 of the EGFP Nb- or Nb5-expressing cells and MK-2206-treated cells. Colocalization coefficients for all other treatments (MK-2206, EGFP Nb and Nb5) were not significantly different. **C:** Western Blot detection of Vinculin (loading control), AKT2 phosphorylated on S474 (**pAKT2 S474**), Cyclin D1, CDK2 and Nb8. **1**= untreated cells, **2**= Dox-treated (500 ng/mL) and **3**= MK-2206-treated (5 μM) MDA-MB-231 cells. Representative for at least six repeated experiments. **D:** Quantification of Cyclin D1 and CDK2 using ImageJ. Values were normalized for vinculin. The fold change for Dox-treated versus untreated cells is plotted. All data points are shown with their mean (**dashed line**) and a 95 % CI (**Whiskers**). * **p < 0.05** and *** **p < 0.001**, Wilcoxon signed rank test. Repeats are available in Supplementary Fig. S10. **E:** Cell cycle phase distribution of Nb-expressing MDA-MB-231 cells. Cells were gated to exclude debris, doublets and to include Nb-expressing cells. Values shown are the mean and SD of at least 3 repeated experiments. The proportion of cells in the G0/G1-, S- and G2-phase is shown as a percentage. Note that the y-axis has a break between 10 % and 60 %.

identified, none of which met the criteria for different regulation. The site identified for AKT3 (S472) is the HM site, corresponding to S474 in AKT2. A total of 20 known AKT substrates were quantified, none of these were differentially regulated between Nb8- and EGFP Nb-expressing cells (Supplementary Table S2). These sites include BAD S99, GSK3β S9 and, a known AKT1 substrate, PALLADIN S1118. A NetPhos motif search identified three potential AKT substrate sites: TRA2A (T88), SRRM1 (S551) and IRS1 (S270), all of which were down-regulated in Nb8-expressing cells [56].

To identify the cellular processes influenced by Nb8 expression, all differentially regulated proteins (phosphorylation and expression) were subjected to PANTHER Gene Ontology (GO) term enrichment and KEGG pathway mapping [57]. A selection of enriched terms is shown in Fig. 5C. Fold enrichment and P-values for all significantly enriched GO terms can be found in the supplementary data. For cellular component, both 'nucleoplasm' and 'cytosol' were enriched while 'integral component of membrane' was underrepresented. This could indicate that our analysis did not equally cover the whole proteome. Interestingly, given the results from the XTT and clonogenic assays, 'mitotic cell cycle' was an enriched biological process term and five proteins were mapped to the KEGG 'cell cycle' pathway. AKT2 inactivation has been linked to autophagy. Proteins involved in autophagy, mitophagy and phagophore assembly site were overrepresented in the significantly regulated proteins. Additionally, seven proteins were mapped to the 'KEGG autophagy – animal' pathway [23,58]. Several terms pertaining to the cytoskeleton and cell motility were enriched including, but not limited to, stress fiber, basement membrane, cell-cell adherens junction, focal adhesion and cytoskeleton. Furthermore, mapping the protein list to KEGG pathways identified seven hits to be part of the 'focal adhesion' pathway and five hits were mapped to the 'actin cytoskeleton' pathway. These results prompted us to investigate the effects of Nb8 on the cell cycle, autophagy and focal adhesions in more detail.

3.2.5. Nb8 interference with AKT2 results in a G0/G1 cell cycle arrest

The AKT family was previously established as a regulator of the cell cycle [59]. In total, the GO enrichment and KEGG pathway mapping yielded 26 proteins (Fig. 5C, Supplementary Table S3) involved in various stages of the mitotic cell cycle or regulation of DNA metabolic processes. Retinoblastoma-associated protein (RB1), a tumour suppressor and regulator of the cell cycle, was hypophosphorylated on multiple sites. These phosphosites were not down-regulated to the same extent and RB1 expression was not significantly (**p > 0.05**) down-regulated in Nb8-expressing cells. With the exception of S37, the identified RB1 phosphosites are regulated by Cyclin D1-CDK4/6 complexes or Cyclin A/E-CDK2 complexes [60].

The localization and degradation of Cyclin D1 is regulated by phosphorylation on T286, downstream of AKT and AKT also regulates Cyclin D1 activity through CDKN1A and CDKN1B [61–63]. Immunofluorescence (IF) and Western blotting were used to determine the effect of Nb8 expression on Cyclin D1. IF experiments showed that Cyclin D1 was enriched in the nucleus (Supplementary Fig. S8) (co-localization with DAPI according to Mander's Colocalization Coefficient quantified

using ImageJ) [64]. This was still the case in MK-2206 (pan-AKT inhibitor)-treated cells and EGFP Nb- or Nb5-expressing cells (Fig. 6A). In cells expressing Nb8, the nuclear enrichment of Cyclin D1 was lost as these cells had a significantly lower overlap between DAPI and Cyclin D1 (one-way ANOVA, **p < 0.001**) (Fig. 6B). No (phospho)peptides for Cyclin D1 were found in the proteomics analyses. Western blotting was used to determine changes in Cyclin D1 protein expression levels. Nb8-expressing cells showed a significant (Wilcoxon signed rank test, **p < 0.001**) reduction in Cyclin D1 levels when compared to the un-induced control (Fig. 6C, D). Again, we found that MK-2206 treatment had no effect on Cyclin D1 even though it strongly reduced AKT2 S474 phosphorylation. A one-way ANOVA with Dunnett's test indicated that there were no significant differences in Cyclin D1 levels between the EGFP Nb-, Nb5- and Nb9-expressing or MK-2206-treated cells. In addition, we found that CDK2 levels were also significantly down-regulated in Nb8-expressing cells (Wilcoxon signed rank test, **p < 0.05**). A cell cycle analysis showed that, compared to the EGFP Nb-expressing cells, the Nb8-expressing cell line had a significantly (one-way ANOVA with Tukey's multiple comparison test, **p < 0.001**) higher proportion of cells in the G0/G1 phase (+**19.36 ±3.43 %**) at the expense of cells in both the S (-**10.22 ± 1.77 %**) and G2 phase (-**8.77 ± 2.77 %**) (Fig. 6E). The cell cycle profile of Nb5- and Nb9-expressing cells was similar to that of EGFP Nb-expressing cells. With the exception of the G2 phase of cells expressing Nb9, which showed a very small (-**3.08 ± 3.06 %**) but significant (**p < 0.05**) decrease, there were no significant differences in population for any cell cycle phase. Full data for the one-way ANOVA with Tukey's post-test can be found in Supplementary Fig. S9.

Although the experiments above focused on signalling events downstream of Cyclin D1-CDK4/6 complexes, CDK2 and the cell cycle entry of MDA-MB-231 cells, there were indications of reduced activity of other cyclin-dependent kinases (CDKs) and reduced phosphorylation of proteins which function in later stages of the cell cycle (Supplementary Table S3). NIFK, an interaction partner of Ki-67, phosphorylation was down-regulated on T234 and T238, substrate sites for GSK3α/β and CDK1, respectively. Although this infers reduced GSK3α/β activity, T234 can only be phosphorylated after CDK1 has phosphorylated T238 [65]. Reduced CDK1 activity would thus result in a reduction of phosphorylation for both these sites. Phosphorylation of both sites is required for the NIFK-Ki-67 interaction. Both proteins are recruited to the chromosome periphery during mitosis [66]. Ki-67, a biomarker for proliferating cells, phosphorylation on S1937, S2223 and T2231 were also reduced. TPX2, a protein involved in cell cycle progression, phosphorylation was down-regulated on S738, another CDK1 substrate site and RRM2, which regulates the synthesis of DNA precursors, was down-regulated on S20 which is a CDK2 substrate site.

Taken together, our other results show that Nb8 expression affected cell cycle progression through inhibition of the AKT2/CyclinD1-CDK2/ RB1 signalling cascade. The final result was a reduction in RB1 phosphorylation on several CDK-dependent sites allowing this protein to exert its tumour suppressive function, i.e. Nb8-expressing cells failed to enter the S-phase.
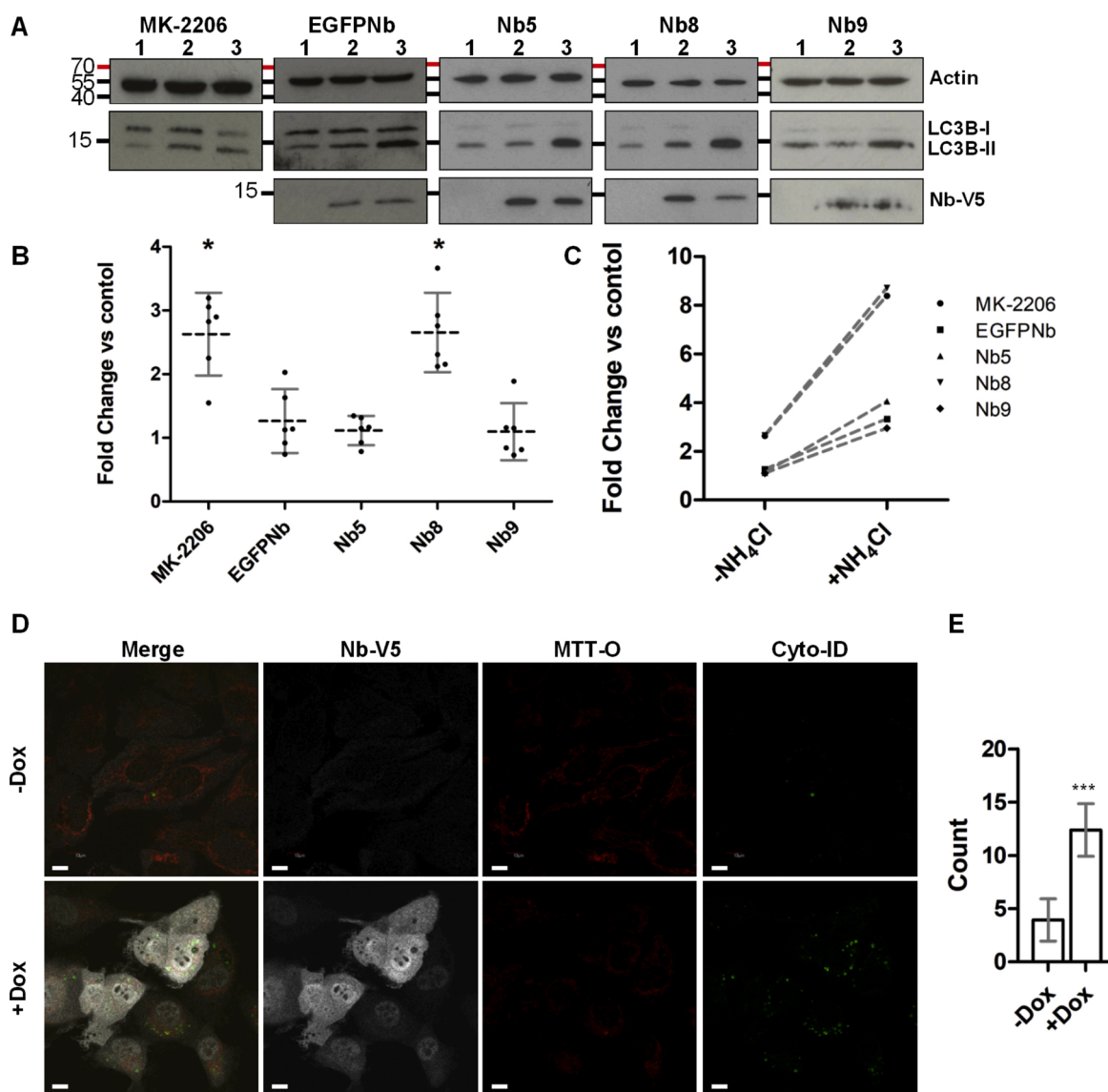
Fig. 7. Nb8 induced autophagy.
A: Western blot detection of LC3B-II. **1**= untreated control, **2**= MK-2206 (5 μM) or Dox (500 ng/mL) for 24 h and **3**= MK-2206 or Dox (24 h) with NH_4Cl (10 mM) added 4 h prior to cell lysis. Actin was used as loading control. The LC3B Ab detected both LC3B-I and LC3B-II. Nbs were detected through their V5-tag. **B:** ImageJ quantification of signal intensity. Values were normalized for the loading control (Actin) and experimental control (uninduced cells). All data points, their mean (**dashed line**) and a 95 % CI (**whiskers**) are shown. Both MK-2206-treated and Nb8-expressing cells showed a significant (*$p < 0.05$, Wilcoxon signed rank test) fold change increase in LC3B-II levels. **C:** Further increase in LC3B-II levels in NH_4Cl-treated cells, indicating that an up-regulation of autophagy rather than inhibition of autophagic flux lies at the base of LC3B-II increase in MK-2206-treated and Nb8-expressing cells. Repeats are available as Supplementary Fig. S11. **D:** representative confocal images of MDA-MB-231 cells. Cells expressing Nb8 contained significantly more autophagosomes (as **green** dots, Cyto-ID). Mitochondria were stained using Mitotracker® Orange CMTMRos (**red**). Autophagosomes were located near the mitochondrial network in both Nb8-expressing and un-induced cells. Scale bar, 20 μm. **E:** Average amount (mean and 95 % CI) of autophagic vesicles per cell from at least 200 cells spread over three repeated experiments. Nb8-expressing cells had significantly (*** $p < 0.0001$) more autophagic vesicles per cell.

3.2.6. Nb8 activates autophagy

Previous studies indicated that ablation of AKT2 induces autophagy [23]. Autophagy (and mitophagy) were enriched biological processes identified in our proteomics analysis along with the cellular component 'phagophore assembly site'. Pooling the hits from these GO keywords yielded 12 proteins with 14 differentially regulated phosphosites and four proteins with significant changes in expression levels (Fig. 5C, Supplementary Table S4). One of those proteins, Transcription factor EB (TFEB), controls expression of autophagy-related and lysosomal genes, among which are MAP1LC3B (LC3B) and ATG9A. TFEB is phosphorylated by mTORC1 on S122 and S142, resulting in the cytoplasmatic

retention and inactivation of TFEB [67,68]. Both of these sites were down-regulated in Nb8-expressing cells along with S109, S114 and S138, the former two of which have also been shown to regulate TFEB localization. Additionally, RBC1CC1/FIP200, an integral part of the ULK complex, phosphorylation on S222 was up-regulated as were phosphorylation sites of MAP1B (S541, S1785, T1788 and S2211), while both ATG2B (S497) and ATG9A (S656) phosphorylation were down-regulated. The effect of these PTMs for RB1CC1, MAP1B, ATG2B and ATG9A is unknown, but these proteins are involved in autophagosome formation, ATG2B and ATG9A in the early stages and RB1CC1/FIP200 in both early and late stages. Phosphorylated MAP1B
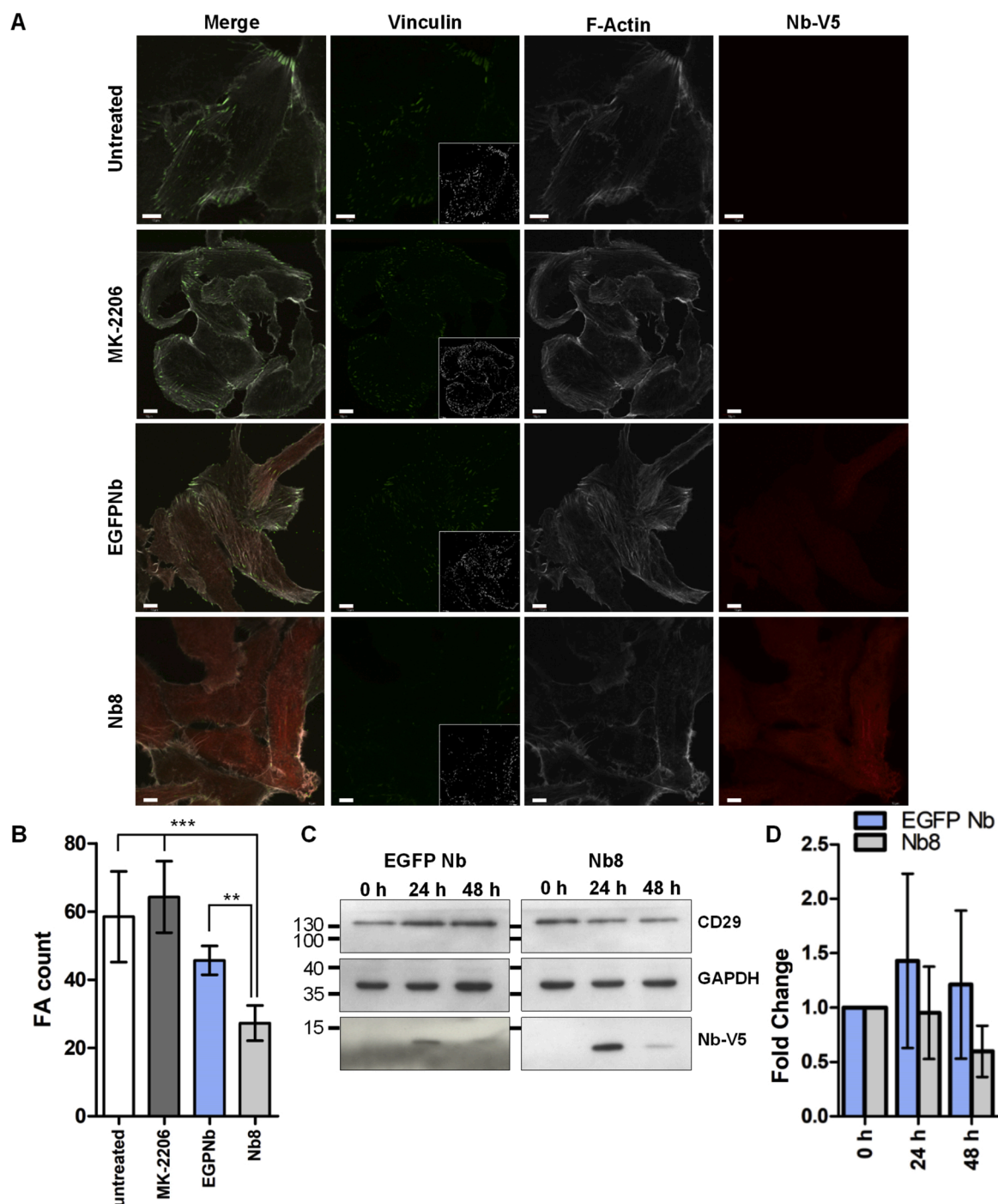
Fig. 8. Nb8 reduced the number of Focal Adhesions present in MDA-MB-231 cells.
A: representative confocal images of MDA-MB-231 cells. Vinculin was used as a marker for Focal adhesions, actin filaments and Nbs were visualised using fluorescent phalloidin and an anti-V5 Ab, respectively. Focal adhesions are visible as green vinculin streaks at the ends of actin filaments. Nb8-expressing cells contained both less vinculin streaks and fewer structured actin filaments when compared to the control conditions. Vinculin image insets are after background subtraction and thresholding [51]. Scale bar, 20 μm. **B:** ImageJ quantification of FAs for at least 100 cells. ** $p < 0.01$, ***$p < 0.001$. **C:** Western blot detection of CD29 in MDA-MB-231 cells expressing the EGFP Nb-(control) or Nb8. Nb expression was induced by 500 ng/mL Dox for up to 48 h. GAPDH was used as loading control, the Nbs were detected through their V5-tag. **D:** ImageJ quantification of signal intensity for CD29, normalized for GAPDH. Repeats are available as Supplementary Fig. S12. A one-way ANOVA with dunnett's multiple comparison test showed that, after 48 h of Nb8 expression, CD29 levels were significantly reduced (**$p < 0.05$**).

interacts with LC3B and links autophagosomes to microtubuli [69,70].

To determine whether these changes induced autophagy in Nb8-expressing cells we analysed the levels of LC3B-II. The precursor protein LC3B is cleaved to form LC3B-I which, on induction of autophagy, is lipidated (phosphatidylethanolamine conjugation) to LC3B-II. This lipidated form migrates faster in SDS-PAGE and can be used as a marker for autophagy (Fig. 7A) [71]. LC3B-II levels were significantly up-regulated in Nb8-expressing cells and MK-2206-treated cells ($p < 0.05$, Wilcoxon signed rank test) when compared to the un-induced or untreated cells (Fig. 7B). The fold change in LC3B-II levels (normalized for their respective control) of Nb8-expressing cells or MK-2206-treated cells was not significantly different ($p = 0.84$). An additional control, where NH_4Cl is added to the medium of treated cells, was included to ensure LC3B-II up-regulation was due to increased autophagy and not inhibition of autophagic flux (downstream processing of autophagic cargo). NH_4Cl prevents lysosomal acidification and the further increase of LC3B-II in doubly-treated (Dox + NH_4Cl or MK-2206+NH_4Cl) cells indicated that MK-2206-treatment or Nb8 expression did not block autophagic flux (Fig. 7C). The increased presence of autophagosomes in Nb8-expressing cells was confirmed though confocal microscopy using the Cyto-ID® dye (Fig. 7D). Mitochondria were stained using Mito-Tracker® Orange CMTMRos and Nb8 was visualized through its V5-tag. The average amount of autophagic vesicles per cell was determined through ImageJ quantification. A Mann Whitney test indicated that Nb8-expressing cells contained significantly more autophagic vesicles ($p < 0.0001$) (Fig. 7E).

Nb8 expression affected the phosphorylation status and expression levels of several proteins involved in autophagy. The observed LC3B-II upregulation and the higher amount of autophagic vesicles clearly shows the activation of autophagy as a result of Nb8 expression.

3.2.7. Nb8 reduces focal adhesion count and CD29 expression

In breast cancer cells, AKT1 and AKT2 have opposing effects on cell migration and metastasis, AKT1 activity reduces, while AKT2 enhances these processes. Our data indicated that Nb8 expression changes phosphorylation and/or expression levels of multiple proteins involved in cell adhesion and motility (Fig. 5C, Supplementary Table S5). Cell motility requires the dynamic remodeling of the cytoskeleton, including actin stress fibers and focal adhesions [72]. Focal adhesions (FA) are large protein complexes that link the extracellular matrix to the actin cytoskeleton through transmembrane integrins. In total, 17 and 7 differentially regulated proteins were quantified that localize to FAs and stress fibers, respectively.

The effect of these changes in protein expression and phosphorylation on FAs in MDA-MB-231 cells was determined through IF, using Vinculin as a marker for FAs and labelled phalloidin to visualize F-actin (Fig. 8A) [73]. FAs were quantified using ImageJ, the data are representative for three repeated experiments with at least 100 cells for each treatment. A one-way ANOVA (with Dunnett's multiple comparison test) indicated that cells expressing Nb8 had significantly fewer FAs ($p < 0.01$ for EGFP Nb vs Nb8 and $p < 0.001$ for untreated and MK-2206-treated cells vs Nb8) (Fig. 8B). Peptides from Vinculin were identified in the SG proteomics analysis. LFQ indicated that Vinculin expression levels were unchanged for Nb8- vs EGFP Nb-expressing cells, suggesting that Vinculin is displaced from FAs. Additionally, Nb8-expressing cells contained fewer structured actin filaments.

The expression of Integrin β1 (CD29), an integral part of FAs, is up-regulated by AKT2 and promotes breast cancer cell migration [20,33]. WB detection of CD29 showed CD29 levels were reduced in MDA-MB-231 cells after 48 h of Nb8 expression (Fig. 8C) (one-way ANOVA with Dunnett's multiple comparison test, $p < 0.05$) (Fig. 8D). For the EGFP Nb-expressing cells no significant differences in CD29 levels were found for any time point.

4. Discussion

In a previous study, we obtained and characterised three AKT2 specific Nbs (Nb5, Nb8 and Nb9) which interact with the catalytic, HM and PH domain of AKT2, respectively [50]. Nbs can knock out specific protein functions without reducing protein expression levels [42–46,48, 49,74]. This makes Nbs complementary tools to RNAi for studying protein function. However, a function-blocking Nb seems to be a better indicator of the effects of a conventional inhibitor and such Nbs (or their therapeutic epitope) can be used in the discovery or design of new inhibitors. Here, we present high-affinity AKT2-interactors that can be used in living cells. Through lentiviral transduction, the AKT2 Nbs were stably integrated into the genome of MDA-MB-231 cells and can pull-down endogenous AKT2.

Nb9 has been shown to interfere with the interaction of the AKT2 PH-domain with PtdIns(3,4,5)P_3 which, in theory, could affect AKT2 activation. However, despite the results from cell-free experiments, we did not observe a reduction in AKT2 HM phosphorylation in IGF-1 stimulated cells expressing Nb9. The cell-free experiments did use a high molar excess of Nb9 over PH-domain. Nb9 has a higher affinity for the AKT2 PH-domain when compared to PtdIns(3,4,5)P_3 (583 pM vs 590 nM), but perhaps Nb9 expression levels were too low to overcome the sudden spike in local PtdIns(3,4,5)P_3 concentration [75,76].

We found that Nb8 expression reduces phosphorylation of AKT2's HM (S474) in IGF-1-stimulated cells. As Nb8 binds the HM and reduces, but not abolishes, phosphorylation of that domain it is likely that Nb8 does not completely inhibit AKT2 function. Phosphorylation of the AKT HM has been shown to 'fine tune' AKT signalling, a reduction in phosphorylation of this site only affects a subpopulation of AKT substrates [35,54,55]. Nb8's effect is not necessarily limited to reducing the catalytic activity of AKT2. The interaction of Nb8 with the AKT2 HM could block 'structural' AKT2 functions. It could restrict access to specific AKT2 substrates or interfere with the interaction of AKT2-regulating proteins [44–46,49,74,77]. A phosphoproteome analysis reliably quantified 7,677 phosphosites, 189 of which were differentially regulated between Nb8- and EGFP Nb-expressing cells. The shotgun proteome analysis of the same samples quantified 2,509 proteins, 37 of these had significant changes in expression levels. The AKT3 HM phosphosite (S472) was quantified but not down-regulated in Nb8-expressing cells, which was expected as Nb8 does not interact with this isoform. The corresponding phosphosites for AKT1 and AKT2 were not quantified, nor was the phosphosite in the catalytic domain identified for any isoform. That several AKT substrate sites were quantified but not differentially regulated indicates that these are either not AKT2-specific substrates or that their phosphorylation is not affected by a reduction of AKT2 HM phosphorylation. The phosphorylation status of T309 and S474 (residues for AKT2) has been suggested to determine substrate accessibility. Singly phosphorylated AKT at T309 would retain most of its functions, while doubly phosphorylated AKT (T309 and S474) adds additional substrates to its repertoire [54,55]. It remains to be seen whether this additional level in AKT regulation is also isoform-specific [12,35,54]. That no known AKT substrates were differentially regulated also means that we were unable to find a direct link between AKT2 and the differentially regulated phosphosites or proteins based on previously identified AKT substrates (PhosphoSitePlus). That the novel potential AKT substrates identified by a NetPhos sequence motif search were all down-regulated could indicate these are regulated by AKT2 and that they are affected by Nb8.

BAD S99 is an example of an AKT substrate site that is unaffected by Nb8 expression. This is in line with our observation that Nb8 did not induce apoptosis, as shown by the lack of caspase-3 processing. This shows that AKT2 does not play a dominant role in the regulation of apoptosis in the breast cancer model used here. However, the roles of the

AKT isoforms in regulating apoptosis are most likely context-dependent. There are reported cases where knockdown of a single isoform was sufficient to induce apoptosis, but also where a combined knockdown of all isoforms was required to obtain a similar effect [2,30].

The AKT kinases are part of a large network that includes multiple kinases downstream of AKT [5]. We expected that the majority of the identified phosphosites would be indirectly regulated by AKT2. A Fisher exact test on substrate motifs for differentially regulated phosphosites showed consensus phosphorylation sites for CHK1, CAMK2, CAMK4, PKA and PKC were enriched. The AKT pathway also includes several transcription factors, 17 differentially regulated proteins have 'transcription regulation' as UniProtKB keyword (Appendix ASupplementary Proteomics Data). Proteins of which the expression levels were significantly altered add another layer of information to the effect of AKT2 modulation by Nb8.

GO term analysis and KEGG pathway mapping linked the differentially regulated proteins (both phosphorylation and expression levels) to specific functions regulated by AKT2. Indeed, the vast majority of our protein hits are involved in processes known to be regulated by the AKT family [20,21,23,32,39,58,78]. Our results implicate AKT2 as the dominant isoform in cell cycle regulation. Phosphorylation levels of GSK3β, an AKT substrate that phosphorylates Cyclin D1 on T286 inducing nuclear export, were unchanged. This indicates that GSK3β is not responsible for the reduction in Cyclin D1 expression levels which is in line with results from a study using AKT2 siRNA [23]. There are other kinases downstream of AKT, such as DYRK1B and IKKA, which can also phosphorylate this site [79,80]. Additionally, this effect could also be achieved by the inhibition of Cyclin D1-CDK4 complexes by CDKN1A or CDKN1B, both direct AKT substrates. CDKN1B upregulation has been observed in MDA-MB-231 cells with AKT2 down-regulation through siRNA [23,61]. The downregulation of Cyclin D1 and CDK2 accounts for the hypophosphorylation of seven out of eight detected RB1 phosphosites. These changes enable RB1 to exert its tumour suppressive functions. That not all phosphosites were down-regulated to the same extent suggests that there may be other upstream elements involved in RB1 regulation that are also affected by Nb8. Ten RB1 transcription targets that play a role in the cell cycle were quantified by shotgun proteomics. Only three (MCM6, RRM1 and CDK1) were significantly down-regulated, but the fold change was too low to be considered biologically relevant [60]. Treating cells with MK-2206, a pan-AKT inhibitor, did not reduce Cyclin D1 or CDK2 levels. Another study has shown that MK-2206 treatment does not affect cell cycle progression in MDA-MB-231 cells [53]. Our results show this cell type is sensitive to AKT2 inhibition, resulting in a G0/G1 cell cycle arrest. This raises the question why AKT2 inhibition affects cell cycle progression, but full inhibition of the AKT family does not. Both AKT1 and AKT2 have been shown to regulate Cyclin D1 expression levels in MDA-MB-231 cells, which makes it unlikely that regulation of this process is AKT2-specific [23]. It is possible that complete inhibition of the AKT family triggers feedback mechanisms which are not activated by a reduction in AKT2 activity alone [81,82].

Contrary to the effects on cell cycle progression, both Nb8 and MK-2206 had equal effects on induction of autophagy in MDA-MB-231 cells, specifically LC3B-II up-regulation. This indicates that neither AKT1 nor AKT3 plays a significant role in this process as inhibition of these kinases along with AKT2 (in MK-2206-treated cells) did not have an additive effect on LC3B-II levels. Although this was not observed directly, the reduced phosphorylation of TFEB (and EEF2K) sites suggests reduced mTORC1 activity, the main regulator of autophagy downstream of AKT. This is supported by the reduced RPS6KA1 S363 phosphorylation, an upstream activator of mTORC1. In addition to this, we observed increased phosphorylation of RB1CC1/FIP200 and MAP1B,

and reduced phosphorylation of ATG2B and ATG9A. We suggest these modifications play a role in autophagy regulation, although how these are linked to AKT2 remains to be elucidated. Autophagy in cancer is a double-edged sword as it can promote cell survival or cell death [83]. The uncontrolled autophagy induced by Nb8 can lead to cell death and contribute to the effect on cell viability/proliferation. Other studies have shown that AKT2 inhibition leads to targeted degradation of mitochondria by autophagy (mitophagy) [23]. However, we found that autophagosomes stained by Cyto-ID™ were localized to the mitochondrial networks regardless of Nb8 expression (although these were much fewer in number in uninduced cells) and were unable to confirm increased mitochondrial volume in these cells. However, these results were based on knock-down of AKT2 and the time points for evaluation of the effects differ greatly from our own. It is possible that the effect is not yet detectable or that Nb8 specifically blocks certain AKT2 functions and elicits different effects than an AKT2 knockdown.

The role of AKT2 in breast cancer cell migration and metastasis has been well established [20,21,27,28,33,39]. GO term analysis of differentially regulated proteins identified several enriched cellular components, biological processes and molecular functions related to the actin cytoskeleton and cell migration. The phoshorylation of ZYX S308 and PARVA S4/8 is known to affect cell migration, but the function of the majority of the phosphosites identified in our experiments has not yet been elucidated [84,85]. Our results show AKT2 modulation by Nb8 affects FAs in MDA-MB-231 cells. Organized complexes of FAs and stress fibers, which are observed at the leading edge of migrating cells, are not found in Nb8-expressing cells but were still present in MK-2206-treated cells. Although the down-regulation of PALLADIN, as was observed in AKT2 ablated cells, could explain the loss of stress fibers, PALLADIN levels were unchanged in Nb8-expressing cells (Supplementary Fig. S13). This suggests that maintaining PALLADIN expression does not require full AKT2 activity and that a full protein knockdown is required to elicit this effect. It also appears that a complete inhibition of the AKT family by MK-2206 does not have the same effect on the cytoskeleton in MDA-MB-231 cells, which is likely due to the opposite functions of AKT1 and AKT2 in breast cancer cell migration. These results help explain how AKT2-specific signalling promotes cell migration in breast cancer cells.

5. Conclusions

In this study we have used a novel approach to interfere with AKT2. An isoform-specific Nb, which targets the HM, enabled us to study the effect of AKT2 modulation in cells without affecting AKT2 expression levels. The HM is, to our knowledge, a previously unexplored epitope for AKT inhibition. Here, we show the importance of the HM in AKT2 signalling and the cellular processes affected by blocking this domain (Fig. 9). Using high-throughput proteomics approaches we were able to identify proteins regulated by AKT2 further downstream in the pathway and the cellular processes which were affected by Nb8's modulation of AKT2 activity. We show that, in MDA-MB-231 cells, AKT2 is the dominant isoform in cell cycle regulation but, given the results from other studies, think it is unlikely that this process is regulated solely by AKT2. We confirmed AKT2's role in autophagy and identified PTM events that occur on induction of autophagy. Finally, we identified an isoform-specific mechanism by which AKT2 regulates focal adhesions, which could affect the ability of cancer cells to migrate and metastasise. In summary, our results confirm AKT2 and the HM as a bona-fide target for cancer therapy. In contrast to techniques that down-regulate protein expression, Nb8 or its epitope can aid in the rational development of an AKT2-specific inhibitor or be used in the screening for small-molecules that target the AKT2 HM [86,87].
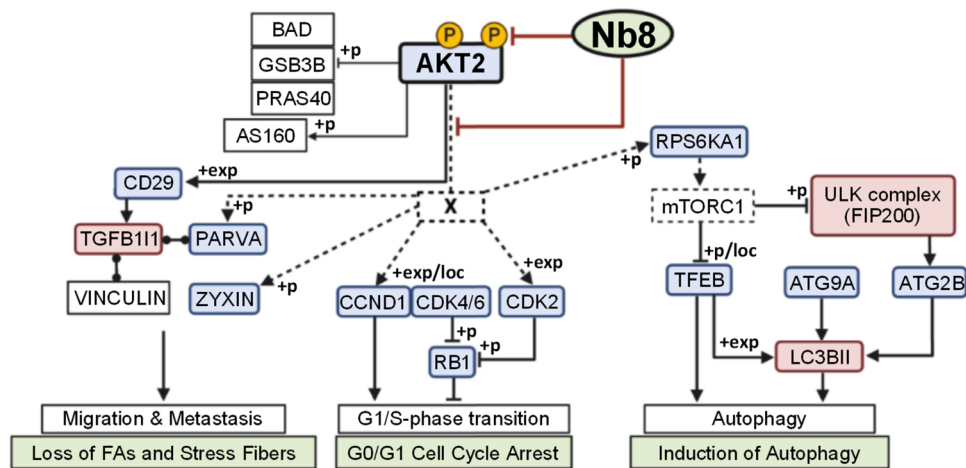
Fig. 9. Summary of Nb8's effects on AKT2 signalling.

A proposed model for the effects of Nb8 in MDA-MB-231 cells based on the results from this study, KEGG, Reactome pathways and STRING interactions. A dashed line indicates events that were not detected in this study, but are known to be a part of the AKT signalling pathway. The box marked "X" indicates the missing link(s) between AKT and the differentially regulated proteins. An arrow and t-bar indicate activating and inhibiting modifications, respectively. Lines ending in dots indicate a protein-protein interaction. $+p$ = phosphorylation, $+exp$ = increased expression and **loc** = effects on localization. White boxes indicate proteins that were detected in our experiments but were not differentially regulated. Red and blue colored boxes indicate detected proteins with up- or down-regulated phosphorylation/expression levels, respectively. The effect of Nb8 on the pathways is shown in a green box at the bottom of the figure. Created using Path-Visio (v. 3.3.0).

Declaration of Competing Interest

J.G. is shareholder of Gulliver Biomed BV. J.G. declares that he has no non-financial competing interests. T.M., O.Z. and K.G. declare no potential conflicts of interest.

Appendix A. Supplementary data

Supplementary material related to this article can be found, in the online version, at doi:https://doi.org/10.1016/j.biopha.2020.111055.

References

[1] M.S. Lawrence, P. Stojanov, C.H. Mermel, J.T. Robinson, L.A. Garraway, T. R. Golub, M. Meyerson, S.B. Gabriel, E.S. Lander, G. Getz, Discovery and saturation analysis of cancer genes across 21 tumour types, Nature 505 (2014) 495–+, https://doi.org/10.1038/nature12912.

[2] M.Q. Song, A.M. Bode, Z.G. Dong, M.H. Lee, AKT as a therapeutic target for Cancer, Cancer Res. 79 (2019) 1019–1031, https://doi.org/10.1158/0008-5472.can-18-2738.

[3] J. Wang, W. Zhao, H.F. Guo, Y. Fang, S.E. Stockman, S. Bai, P.K.S. Ng, Y. Li, Q. H. Yu, Y.L. Lu, K.J. Jeong, X.H. Chen, M. Gao, J.Y. Liang, W.T. Li, X.S. Tian, E. Jonasch, G.B. Mills, Z.Y. Ding, AKT isoform-specific expression and activation across cancer lineages, BMC Cancer 18 (2018) 10, https://doi.org/10.1186/s12885-018-4654-5.

[4] G. Hoxhaj, B.D. Manning, The PI3K-AKT network at the interface of oncogenic signalling and cancer metabolism, Nat. Rev. Cancer 20 (2020) 74–88, https://doi.org/10.1038/s41568-019-0216-7.

[5] B.D. Manning, A. Toker, AKT/PKB Signaling: Navigating the Network, Cell. 169 (2017) 381–405, https://doi.org/10.1016/j.cell.2017.04.001.

[6] X.L. Zhang, S.W. Zhang, H. Yamane, R. Wahl, A. Ali, J.A. Lofgren, R.L. Kendall, Kinetic mechanism of AKT/PKB enzyme family, J. Biol. Chem. 281 (2006) 13949–13956, https://doi.org/10.1074/jbc.M601384200.

[7] M. Ebner, I. Lucic, T.A. Leonard, I. Yudushkin, PI(3,4,5)P-3 engagement restricts akt activity to cellular membranes, Mol. Cell 65 (2017), https://doi.org/10.1016/j.molcel.2016.12.028, 416–+.

[8] N.N. Jiang, Q.J. Dai, X.R. Su, J.J. Fu, X.C. Feng, J. Peng, Role of PI3K/AKT pathway in cancer: the framework of malignant behavior, Mol. Biol. Rep. (2020) 43, https://doi.org/10.1007/s11033-020-05435-1.

[9] L.R. Molife, L. Yan, J. Vitfell-Rasmussen, A.M. Zernhelt, D.M. Sullivan, P.A. Cassier, E. Chen, A. Biondo, E. Tetteh, L.L. Siu, A. Patnaik, K.P. Papadopoulos, J.S. de Bono, A.W. Tolcher, S. Minton, Phase 1 trial of the oral AKT inhibitor MK-2206 plus carboplatin/paclitaxel, docetaxel, or erlotinib in patients with advanced solid tumors, J. Hematol. Oncol. 7 (2014) 12, https://doi.org/10.1186/1756-8722-7-1.

[10] R. Dienstmann, J. Rodon, V. Serra, J. Tabernero, Picking the point of inhibition: a comparative review of PI3K/AKT/mTOR pathway inhibitors, Mol. Cancer Ther. 13 (2014) 1021–1031, https://doi.org/10.1158/1535-7163.mct-13-0639.

[11] A.J. Chien, D. Tripathy, K.S. Albain, W.F. Symmans, H.S. Rugo, M.E. Melisko, A. M. Wallace, R. Schwab, T. Helsten, A. Forero-Torres, E. Stringer-Reasor, E.D. Ellis, H.G. Kaplan, R. Nanda, N. Jaskowiak, R. Murthy, C. Godellas, J.C. Boughey, A. D. Elias, B.B. Haley, K. Kemmer, C. Isaacs, A.S. Clark, J.E. Lang, J. Lu, L. Korde, K. K. Edmiston, D.W. Northfelt, R.K. Viscusi, D. Yee, J. Perlmutter, N.M. Hylton, L. J. van't Veer, A. DeMichele, A. Wilson, G. Peterson, M.B. Buxton, M. Paoloni, J. Clennell, S. Berry, J.B. Matthews, K. Steeg, R. Singhrao, G.L. Hirst, A. Sanil, C. Yau, S.M. Asare, D.A. Berry, L.J. Esserman, I.S. Consortium, MK-2206 and standard neoadjuvant chemotherapy improves response in patients with human epidermal growth factor receptor 2-Positive and/or hormone receptor-negative breast cancers in the I-SPY 2 trial, J. Clin. Oncol. 38 (2020), https://doi.org/10.1200/jco.19.01027, 1059–+.

[12] J. Yang, P. Cron, V.M. Good, V. Thompson, B.A. Hemmings, D. Barford, Crystal structure of an activated Akt/protein kinase B ternary complex with GSK3-peptide and AMP-PNP, Nat. Struct. Biol. 9 (2002) 940–944, https://doi.org/10.1038/nsb870.

[13] L.R. Pearce, D. Komander, D.R. Alessi, The nuts and bolts of AGC protein kinases, Nat. Rev. Mol. Cell Biol. 11 (2010) 9–22, https://doi.org/10.1038/nrm2822.

[14] Y.C. Lai, Y. Liu, R. Jacobs, M.H. Rider, A novel PKB/Akt inhibitor, MK-2206, effectively inhibits insulin-stimulated glucose metabolism and protein synthesis in isolated rat skeletal muscle, Biochem. J. 447 (2012) 137–147, https://doi.org/10.1042/bj20120772.

[15] NIH, NCBI BLAST, 2020, 2020, https://blast.ncbi.nlm.nih.gov/Blast.cgi?PROGRAM=blastp&PAGE_TYPE=BlastSearch&LINK_LOC=blasthome.

[16] R.M. Easton, H. Cho, K. Roovers, D.W. Shineman, M. Mizrahi, M.S. Forman, V.M. Y. Lee, M. Szabolcs, R. de Jong, T. Oltersdorf, T. Ludwig, A. Efstratiadis, M. J. Birnbaum, Role for Akt3/Protein kinase B gamma in attainment of normal brain size, Mol. Cell. Biol. 25 (2005) 1869–1878, https://doi.org/10.1128/mcb.25.5.1869-1878.2005.

[17] W.S. Chen, P.Z. Xu, K. Gottlob, M.L. Chen, K. Sokol, T. Shiyanova, I. Roninson, W. Weng, R. Suzuki, K. Tobe, T. Kadowaki, N. Hay, Growth retardation and increased apoptosis in mice with homozygous disruption of the akt1 gene, Genes Dev. 15 (2001) 2203–2208, https://doi.org/10.1101/gad.913901.

[18] H. Cho, J. Mu, J.K. Kim, J.L. Thorvaldsen, Q.W. Chu, E.B. Crenshaw, K.H. Kaestner, M.S. Bartolomei, G.I. Shulman, M.J. Birnbaum, Insulin resistance and a diabetes mellitus-like syndrome in mice lacking the protein kinase Akt2 (PKB beta), Science (80-.) 292 (2001) 1728–1731, https://doi.org/10.1126/science.292.5522.1728.

[19] Y.R. Chin, A. Toker, The actin-bundling protein palladin is an Akt1-Specific substrate that regulates breast Cancer cell migration, Mol. Cell 38 (2010) 333–344, https://doi.org/10.1016/j.molcel.2010.02.031.

[20] Y.R. Chin, A. Toker, Akt2 regulates expression of the actin-bundling protein palladin, FEBS Lett. 584 (2010) 4769–4774, https://doi.org/10.1016/j.febslet.2010.10.056.

[21] M. Riggio, M.C. Perrone, M.L. Polo, M.J. Rodriguez, M. May, M. Abba, C. Lanari, V. Novaro, AKT1 and AKT2 isoforms play distinct roles during breast cancer

progression through the regulation of specific downstream proteins, Sci. Rep. 7 (2017) 12, https://doi.org/10.1038/srep44244.

[22] E. Agarwal, C.M. Robb, L.M. Smith, M.G. Brattain, J. Wang, J.D. Black, S. Chowdhury, Role of Akt2 in regulation of metastasis suppressor 1 expression and colorectal cancer metastasis, Oncogene 36 (2017) 3104–3118, https://doi.org/10.1038/onc.2016.460.

[23] S.A. Santi, H. Lee, Ablation of Akt2 induces autophagy through cell cycle arrest, the downregulation of p70S6K, and the deregulation of mitochondria in MDA-MB231 cells, PLoS One 6 (2011) 15, https://doi.org/10.1371/journal.pone.0014614.

[24] M.W. Lee, D.S. Kim, J.H. Lee, B.S. Lee, S.H. Lee, H.L. Jung, K.W. Sung, H.T. Kim, K. H. Yoo, H.H. Koo, Roles of AKT1 and AKT2 in non-small cell lung cancer cell survival, growth, and migration, Cancer Sci. 102 (2011) 1822–1828, https://doi.org/10.1111/j.1349-7006.2011.02025.x.

[25] R. Gherzi, M. Trabucchi, M. Ponassi, I.E. Gallouzi, M.G. Rosenfeld, P. Briata, Akt2-mediated phosphorylation of Pitx2 controls Ccnd1 mRNA decay during muscle cell differentiation, Cell Death Differ. 17 (2010) 975–983, https://doi.org/10.1038/cdd.2009.194.

[26] S.A. Santi, H. Lee, The Akt isoforms are present at distinct subcellular locations, Am. J. Physiol. Physiol. 298 (2010) C580–C591, https://doi.org/10.1152/ajpcell.00375.2009.

[27] R.L. Dillon, R. Marcotte, B.T. Hennessy, J.R. Woodgett, G.B. Mills, W.J. Muller, Akt1 and Akt2 play distinct roles in the initiation and metastatic phases of mammary tumor progression, Cancer Res. 69 (2009) 5057–5064, https://doi.org/10.1158/0008-5472.can-08-4287.

[28] J.N. Wang, W.Z. Wan, R.H. Sun, Y. Liu, X.J. Sun, D.L. Ma, N. Zhang, Reduction of Akt2 expression inhibits chemotaxis signal transduction in human breast cancer cells, Cell. Signal. 20 (2008) 1025–1034, https://doi.org/10.1016/j.cellsig.2007.12.023.

[29] I.G. Maroulakou, W. Oemler, S.P. Naber, P.N. Tsichlis, Akt1 ablation inhibits, whereas Akt2 ablation accelerates, the development of mammary adenocarcinomas in mouse mammary tumor virus (MMTV)-ErbB2/Neu and MMTV-polyoma middle T transgenic mice, Cancer Res. 67 (2007) 167–177, https://doi.org/10.1158/0008-5472.can-06-3782.

[30] S. Koseoglu, Z.M. Lu, C. Kumar, P. Kirschmeier, J. Zou, AKT1, AKT2 and AKT3-dependent cell survival is cell line-specific and knockdown of all three isoforms selectively induces apoptosis in 20 human tumor cell lines, Cancer Biol. Ther. 6 (2007) 755–762, https://doi.org/10.4161/cbt.6.5.3995.

[31] L. Heron-Milhavet, C. Franckhauser, V. Rana, C. Berthenet, D. Fisher, B. A. Hemmings, A. Fernandez, N.J.C. Lamb, Only Akt1 is required for proliferation, while Akt2 promotes cell cycle exit through p21 binding, Mol. Cell. Biol. 26 (2006) 8267–8280, https://doi.org/10.1128/mcb.00201-06.

[32] H.Y. Irie, R.V. Pearline, D. Grueneberg, M. Hsia, P. Ravichandran, N. Kothari, S. Natesan, J.S. Brugge, Distinct roles of Akt1 and Akt2 in regulating cell migration and epithelial-mesenchymal transition, J. Cell Biol. 171 (2005) 1023–1034, https://doi.org/10.1083/jcb.200505087.

[33] M.J. Arboleda, J.F. Lyons, F.F. Kabbinavar, M.R. Bray, B.E. Snow, R. Ayala, M. Danino, B.Y. Karlan, D.J. Slamon, Overexpression of AKT2/protein kinase B beta leads to up-regulation of beta 1 integrins, increased invasion, and metastasis of human breast and ovarian cancer cells, Cancer Res. 63 (2003) 196–206.

[34] A.E. Cariaga-Martinez, P. Lopez-Ruiz, M.P. Nombela-Blanco, O. Motino, A. Gonzalez-Corpas, J. Rodriguez-Ubreva, M.V.T. Lobo, M.A. Cortes, B. Colas, Distinct and specific roles of AKT1 and AKT2 in androgen-sensitive and androgen-independent prostate cancer cells, Cell. Signal. 25 (2013) 1586–1597, https://doi.org/10.1016/j.cellsig.2013.03.019.

[35] J. Brognard, E. Sierecki, T.Y. Gao, A.C. Newton, PHLPP and a second isoform, PHLPP2, differentially attenuate the amplitude of Akt signaling by regulating distinct Akt isoforms, Mol. Cell 25 (2007) 917–931, https://doi.org/10.1016/j.molcel.2007.02.017.

[36] E.K. Kim, S.J. Yun, J.M. Ha, Y.W. Kim, I.H. Jin, J. Yun, H.K. Shin, S.H. Song, J. H. Kim, J.S. Lee, C.D. Kim, S.S. Bae, Selective activation of Akt1 by mammalian target of rapamycin complex 2 regulates cancer cell migration, invasion, and metastasis, Oncogene 30 (2011) 2954–2963, https://doi.org/10.1038/onc.2011.22.

[37] K.H. Yi, J. Lauring, Recurrent AKT mutations in human cancers: functional consequences and effects on drug sensitivity, Oncotarget 7 (2016) 4241–4251, https://doi.org/10.18632/oncotarget.6648.

[38] Y.R. Chin, A. Toker, Akt isoform-specific signaling in breast cancer uncovering an anti-migratory role of palladin, Cell Adh. Migr. 5 (2011) 211–214, https://doi.org/10.4161/cam.5.3.15790.

[39] P. Gener, D. Rafael, J. Seras-Franzoso, A. Perez, L.A. Pindado, G. Casas, D. Arango, Y. Fernandez, Z.V. Diaz-Riascos, I. Abasolo, S. Schwartz, Pivotal role of AKT2 during dynamic phenotypic change of breast Cancer stem cells, Cancers (Basel) 11 (2019) 18, https://doi.org/10.3390/cancers11081058.

[40] A.R. Clark, A. Toker, Signalling specificity in the Akt pathway in breast cancer, Biochem. Soc. Trans. 42 (2014) 1349–1355, https://doi.org/10.1042/bst20140160.

[41] S. Muyldermans, Nanobodies: natural single-domain antibodies, in: R.D. Kornberg (Ed.), Annu. Rev. Biochem., Vol 82, 2013, pp. 775–797, https://doi.org/10.1146/annurev-biochem-063011-092449. Annual Reviews, Palo Alto.

[42] A. Steels, A. Verhelle, O. Zwaenepoel, J. Gettemans, Intracellular displacement of p53 using transactivation domain (p53 TAD) specific nanobodies, MAbs 10 (2018) 1045–1059, https://doi.org/10.1080/19420862.2018.1502025.

[43] E. Beghein, D. Devriese, E. Van Hoey, J. Gettemans, Cortactin and fascin-1 regulate extracellular vesicle release by controlling endosomal trafficking or invadopodia formation and function, Sci. Rep. 8 (2018) 16, https://doi.org/10.1038/s41598-018-33868-z.

[44] L. Bertier, T. Hebbrecht, E. Mettepenningen, N. De Wit, O. Zwaenepoel, A. Verhelle, J. Gettemans, Nanobodies targeting cortactin proline rich, helical and actin binding regions downregulate invadopodium formation and matrix degradation in SCC-61 cancer cells, Biomed. Pharmacother. 102 (2018) 230–241, https://doi.org/10.1016/j.biopha.2018.03.064.

[45] L. Bertier, C. Boucherie, O. Zwaenepoel, B. Vanloo, M. Van Troys, I. Van Audenhove, J. Gettemans, Inhibitory cortactin nanobodies delineate the role of NTA- and SH3-domain-specific functions during invadopodium formation and cancer cell invasion, FASEB J. 31 (2017) 2460–2476, https://doi.org/10.1096/fj.201600810RR.

[46] T. Hebbrecht, I. Van Audenhove, O. Zwaenepoel, A. Verhelle, J. Gettemane, VCA nanobodies target N- WASp to reduce invadopodium formation and functioning, PLoS One 12 (2017) 19, https://doi.org/10.1371/journal.pone.0185076.

[47] I. Van Audenhove, J. Gettemans, Nanobodies as versatile tools to understand, diagnose, visualize and treat cancer, Ebiomedicine 8 (2016) 40–48, https://doi.org/10.1016/j.ebiom.2016.04.028.

[48] E. Beghein, I. Van Audenhove, O. Zwaenepoel, A. Verhelle, A. De Ganck, J. Gettemans, A new survivin tracer tracks, delocalizes and captures endogenous survivin at different subcellular locations and in distinct organelles, Sci. Rep. 6 (2016) 16, https://doi.org/10.1038/srep31177.

[49] K. Van Impe, J. Bethuyne, S. Cool, F. Impens, D. Ruano-Gallego, O. De Wever, B. Vanloo, M. Van Troys, K. Lambein, C. Boucherie, E. Martens, O. Zwaenepoel, G. Hassanzadeh-Ghassabeh, J. Vandekerckhove, K. Gevaert, L.A. Fernandez, N. N. Sanders, J. Gettemans, A nanobody targeting the F-actin capping protein CapG restrains breast cancer metastasis, Breast Cancer Res. 15 (2013) 15, https://doi.org/10.1186/bcr3585.

[50] J. Gettemans, T. Merckaert, O. Zwaenepoel, K. Gevaert, Development and characterization of Protein Kinase B/AKT isoform-specific Nanobodies, Res. Sq. (2020), https://doi.org/10.21203/rs.3.rs-18280/v1 (n.d.).

[51] B.O. utku, Horzum Devrim Peden-Okvur, Step-by-step quantitative analysis of focal adhesions, MethodsX 1 (2014) 56–59.

[52] C. Chiva, R. Olivella, E. Borras, G. Espadas, O. Pastor, A. Sole, E. Sabido, QCloud: A cloud-based quality control system for mass spectrometry-based proteomics laboratories, PLoS One 13 (2018) 14, https://doi.org/10.1371/journal.pone.0189209.

[53] T. Sangai, A. Akcakanat, H.Q. Chen, E. Tarco, Y. Wu, K.A. Do, T.W. Miller, C. L. Arteaga, G.B. Mills, A.M. Gonzalez-Angulo, F. Meric-Bernstam, Biomarkers of response to akt inhibitor MK-2206 in breast Cancer, Clin. Cancer Res. 18 (2012) 5816–5828, https://doi.org/10.1158/1078-0432.ccr-12-1141.

[54] E. Jacinto, V. Facchinetti, D. Liu, N. Soto, S.N. Wei, S.Y. Jung, Q.J. Huang, J. Qin, B. Su, SIN1/MIP1 maintains rictor-mTOR complex integrity and regulates Akt phosphorylation and substrate specificity, Cell 127 (2006) 125–137, https://doi.org/10.1016/j.cell.2006.08.033.

[55] D.A. Guertin, D.M. Stevens, C.C. Thoreen, A.A. Burds, N.Y. Kalaany, J. Moffat, M. Brown, K.J. Fitzgerald, D.M. Sabatini, Ablation in mice of the mTORC components raptor, rictor, or mLST8 reveals that mTORC2 is required for signaling to Akt-FOXO and PKC alpha but not S6K1, Dev. Cell 11 (2006) 859–871, https://doi.org/10.1016/j.devcel.2006.10.007.

[56] N. Blom, T. Sicheritz-Ponten, R. Gupta, S. Gammeltoft, S. Brunak, Prediction of post-translational glycosylation and phosphorylation of proteins from the amino acid sequence, Proteomics 4 (2004) 1633–1649, https://doi.org/10.1002/pmic.200300771.

[57] H.Y. Mi, A. Muruganujan, X.S. Huang, D. Ebert, C. Mills, X.Y. Guo, P.D. Thomas, Protocol Update for large-scale genome and gene function analysis with the PANTHER classification system (v.14.0), Nat. Protoc. 14 (2019) 703–721, https://doi.org/10.1038/s41596-019-0128-8.

[58] E.H. Kim, Y. Jo, S. Sai, M.J. Park, J.Y. Kim, J.S. Kim, Y.J. Lee, J.M. Cho, S.Y. Kwak, J.H. Baek, Y.K. Jeong, J.Y. Song, M. Yoon, S.G. Hwang, Tumor-treating fields induce autophagy by blocking the Akt2/miR29b axis in glioblastoma cells, Oncogene 38 (2019) 6630–6646, https://doi.org/10.1038/s41388-019-0882-7.

[59] J.Y. Liang, J.M. Slingerland, Multiple Roles of the PI3K/PKB (Akt) Pathway in Cell Cycle Progression, Cell Cycle 2 (2003) 339–345, https://doi.org/10.4161/cc.2.4.433.

[60] E.S. Knudsen, S.C. Pruitt, P.A. Hershberger, A.K. Witkiewicz, D.W. Goodrich, Cell Cycle and Beyond: Exploiting New RB1 Controlled Mechanisms for Cancer Therapy, Trends Cancer 5 (2019) 308–324, https://doi.org/10.1016/j.trecan.2019.03.005.

[61] B.H.P. Zhou, M.C. Hung, Novel targets of Akt, p21(CipI/WAFI), and MDM2, Semin. Oncol. 29 (2002) 62–70, https://doi.org/10.1053/sonc.2002.34057.

[62] A. Ray, M.K. James, S. Larochelle, R.P. Fisher, S.W. Blain, p27Kip1 inhibits cyclin D-cyclin-dependent kinase 4 by two independent modes, Mol. Cell. Biol. 29 (2009) 986–999, https://doi.org/10.1128/MCB.00898-08.

[63] J.P. Alao, The regulation of cyclin D1 degradation: roles in cancer development and the potential for therapeutic invention, Mol. Cancer 6 (2007) 16, https://doi.org/10.1186/1476-4598-6-24.

[64] K.W. Dunn, M.M. Kamocka, J.H. McDonald, A practical guide to evaluating colocalization in biological microscopy, Am. J. Physiol. 300 (2011) C723–C742, https://doi.org/10.1152/ajpcell.00462.2010.

[65] I.J.L. Byeon, H.Y. Li, H.Y. Song, A.M. Gronenborn, M.D. Tsai, Sequential phosphorylation and multisite interactions characterize specific target recognition by the FHA domain of Ki67, Nat. Struct. Mol. Biol. 12 (2005) 987–993, https://doi.org/10.1038/nsmb1008.

[66] T.C. Lin, C.Y. Su, P.Y. Wu, T.C. Lai, W.A. Pan, Y.H. Jan, Y.C. Chang, C.T. Yeh, C. L. Chen, L.P. Ger, H.T. Chang, C.J. Yang, M.S. Huang, Y.P. Liu, Y.F. Lin, J.Y.J. Shyy, M.D. Tsai, M. Hsiao, The nucleolar protein NIFK promotes cancer progression via

CK1 alpha/beta-catenin in metastasis and Ki-67-dependent cell proliferation, Elife 5 (2016) 21, https://doi.org/10.7554/eLife.11288.

[67] R. Puertollano, S.M. Ferguson, J. Brugarolas, A. Ballabio, The complex relationship between TFEB transcription factor phosphorylation and subcellular localization, EMBO J. 37 (2018) 12, https://doi.org/10.15252/embj.201798804.

[68] C. Settembre, C. Di Malta, V.A. Polito, M. Garcia-Arencibia, F. Vetrini, S. Erdin, S. U. Erdin, T. Huynh, D. Medina, P. Colella, M. Sardiello, D.C. Rubinsztein, A. Ballabio, TFEB links autophagy to lysosomal biogenesis, Science (80-.) 332 (2011) 1429–1433, https://doi.org/10.1126/science.1204592.

[69] B. Harrison, M. Kraus, L. Burch, C. Stevens, A. Craig, P. Gordon-Weeks, T.R. Hupp, DAPK-1 binding to a linear peptide motif in MAP1B stimulates autophagy and membrane blebbing, J. Biol. Chem. 283 (2008) 9999–10014, https://doi.org/10.1074/jbc.M706040200.

[70] Q.J. Wang, Y.M. Ding, S. Kohtz, N. Mizushima, I.M. Cristea, M.P. Rout, B.T. Chait, Y. Zhong, N. Heintz, Z.Y. Yue, Induction of autophagy in axonal dystrophy and degeneration, J. Neurosci. 26 (2006) 8057–8068, https://doi.org/10.1523/jneurosci.2261-06.2006.

[71] D.J. Klionsky, K. Abdelmohsen, A. Abe, M.J. Abedin, H. Abeliovich, A.A. Arozena, H. Adachi, C.M. Adams, P.D. Adams, K. Adeli, P.J. Adhihetty, S.G. Adler, G. Agam, R. Agarwal, M.K. Aghi, M. Agnello, P. Agostinis, P.V. Aguilar, J. Aguirre-Ghiso, E. M. Airoldi, S. Ait-Si-Ali, T. Akematsu, E.T. Akporiaye, M. Al-Rubeai, G. M. Albaiceta, C. Albanese, D. Albani, M.L. Albert, J. Aldudo, H. Algul, M. Alirezaei, I. Alloza, A. Almasan, M. Almonte-Beceril, E.S. Alnemri, C. Alonso, N. Altan-Bonnet, D.C. Altieri, S. Alvarez, L. Alvarez-Erviti, S. Alves, G. Amadoro, A. Amano, C. Amantini, S. Ambrosio, I. Amelio, A.O. Amer, M. Amessou, A. Amon, Z.Y. An, F. A. Anania, S.U. Andersen, U.P. Andley, C.K. Andreadi, N. Andrieu-Abadie, A. Anel, D.K. Ann, S. Anoopkumar-Dukie, M. Antonioli, H. Aoki, N. Apostolova, S. Aquila, K. Aquilano, K. Araki, E. Arama, A. Aranda, J. Araya, A. Arcaro, E. Arias, H. Arimoto, A.R. Ariosa, J.L. Armstrong, T. Arnould, I. Arsov, K. Asanuma, V. Askanas, E. Asselin, R. Atarashi, S.S. Atherton, J.D. Atkin, L.D. Attardi, P. Auberger, G. Auburger, L. Aurelian, R. Autelli, L. Avagliano, M.L. Avantaggiati, L. Avrahami, S. Awale, N. Azad, T. Bachetti, J.M. Backer, D.H. Bae, J.S. Bae, O. N. Bae, S.H. Bae, E.H. Baehrecke, S.H. Baek, S. Baghdiguian, A. Bagniewska-Zadworna, H. Bai, J. Bai, X.Y. Bai, Y. Bailly, K.N. Balaji, W. Balduini, A. Ballabio, R. Balzan, R. Banerjee, G. Banhegyi, H.J. Bao, B. Barbeau, M.D. Barrachina, E. Barreiro, B. Bartel, A. Bartolome, D.C. Bassham, M.T. Bassi, R.C. Bast, A. Basu, M.T. Batista, H. Batoko, M. Battino, K. Bauckman, B.L. Baumgarner, K.U. Bayer, R. Beale, J.F. Beaulieu, G.R. Beck, C. Becker, J.D. Beckham, P.A. Bedard, P. J. Bednarski, T.J. Begley, C. Behl, C. Behrends, G.M.N. Behrns, K.E. Behrns, E. Bejarano, A. Belaid, F. Belleudi, G. Benard, G. Berchem, D. Bergamaschi, M. Bergami, B. Berkhout, L. Berliocchi, A. Bernard, M. Bernard, F. Bernassola, A. Bertolotti, A.S. Bess, S. Besteiro, S. Bettuzzi, S. Bhalla, S. Bhattacharyya, S. K. Bhutia, C. Biagosch, M.W. Bianchi, M. Biard-Piechaczyk, V. Billes, C. Bincoletto, B. Bingol, S.W. Bird, M. Bitoun, I. Bjedov, C. Blackstone, L. Blanc, G.A. Blanco, H. K. Blomhoff, E. Boada-Romero, S. Bockler, M. Boes, K. Boesze-Battaglia, L.H. Boise, A. Bolino, A. Boman, P. Bonaldo, M. Bordi, J. Bosch, L.M. Botana, J. Botti, G. Bou, M. Bouche, M. Bouchecareilh, M.J. Boucher, M.E. Boulton, S.G. Bouret, P. Boya, M. Boyer-Guittaut, P.V. Bozhkov, N. Brady, V.M.M. Braga, C. Brancolini, G. H. Braus, M. Bravo-San Pedro, L.A. Brennan, E.H. Bresnick, P. Brest, D. Bridges, M.A. Bringer, M. Brini, G.C. Brito, B. Brodin, P.S. Brookes, E.J. Brown, K. Brown, H. E. Broxmeyer, A. Bruhat, P.C. Brum, J.H. Brumell, N. Brunetti-Pierri, R.J. Bryson-Richardson, S. Buch, A.M. Buchan, H. Budak, D.V. Bulavin, S.J. Bultman, S. J. Bultman, V. Bumbasirevic, Y. Burelle, R.E. Burke, M. Burmeister, P. Butikofer, L. Caberlotto, K. Cadwell, M. Cahova, D.S. Cai, J.J. Cai, Q. Cai, S. Calatayud, N. Camougrand, M. Campanella, G.R. Campbell, M. Campbell, S. Campello, R. Candau, I. Caniggia, L. Cantoni, L.Z. Cao, A.B. Caplan, M. Caraglia, C. Cardinali, S.M. Cardoso, J.S. Carew, L.A. Carleton, C.R. Carlin, S. Carloni, S.R. Carlsson, D. Carmona-Gutierrez, L.A.M. Carneiro, O. Carnevali, S. Carra, A. Carrier, B. Carroll, C. Casas, J. Casas, G. Cassinelli, P. Castets, S. Castro-Obregon, G. Cavallini, I. Ceccherini, I. Cecconi, A.I. Cederbaum, V. Cena, S. Cenci, C. Cerella, D. Cervia, S. Cetrullo, H. Chaachouay, H.J. Chae, A.S. Chagin, C.Y. Chai, G. Chakrabarti, G. Chamilos, E.Y.W. Chan, M.T.V. Chan, D. Chandra, P. Chandra, C.P. Chang, R.C.C. Chang, T.Y. Chang, J.C. Chatham, S. Chatterjee, S. Chauhan, Y. S. Che, M.E. Cheetham, R. Cheluvappa, C.J. Chen, G. Chen, G.C. Chen, G.Q. Chen, H.Z. Chen, W. Chen, J.K. Chen, M. Chen, M.Z. Chen, P.W. Chen, Q. Chen, Q. Chen, S.D. Chen, S. Chen, S.S.L. Chen, W. Chen, W.J. Chen, W.Q. Chen, W. L. Chen, X.M. Chen, Y.H. Chen, Y.G. Chen, Y. Chen, Y.Y. Chen, Y.S. Chen, Y. J. Chen, Y.Q. Chen, Y.J. Chen, Z. Chen, Z. Chen, A. Cheng, C.H.K. Cheng, H. Cheng, H.S. Cheong, S. Cherry, J. Chesney, C.H.A. Cheung, E. Chevet, H.C. Chi, S.G. Chi, F. Chiacchiera, H.L. Chiang, R. Chiarelli, M. Chiariello, M. Chieppa, L.S. Chin, M. Chiong, G.N.C. Chiu, D.H. Cho, S.G. Cho, W.C. Cho, Y.Y. Cho, Y.S. Cho, A.M. K. Choi, E.J. Choi, E.K. Choi, J.Y. Choi, M.E. Choi, S.I. Choi, T.F. Chou, S. Chouaib, D. Choubey, V. Choubey, K.C. Chow, K. Chowdhury, C.T. Chu, T.H. Chuang, T. Chun, H.W. Chung, T.J. Chung, Y.L. Chung, Y.J. Chwae, V. Cianfanelli, R. Ciarcia, I.A. Ciechomska, M.R. Ciriolo, M. Cirone, S. Claerhout, M.J. Clague, J. Claria, P.G.H. Clarke, R. Clarke, E. Clementi, C. Cleyrat, M. Cnop, E.M. Coccia, T. Cocco, P. Codogno, J. Coers, E.E.W. Cohen, D. Colecchia, L. Coletto, N.S. Coll, E. Colucci-Guyon, S. Comincini, M. Condello, K.L. Cook, G.H. Coombs, C. D. Cooper, J.M. Cooper, I. Coppens, M.T. Corasaniti, M. Corazzari, R. Corbalan, E. Corcelle-Termeau, M.D. Cordero, C. Corral-Ramos, O. Corti, A. Cossarizza, P. Costelli, S. Costes, S. Costes, A. Coto-Montes, S. Cottet, E. Couve, L.R. Covey, L. A. Cowart, J.S. Cox, F.P. Coxon, C.B. Coyne, M.S. Cragg, R.J. Craven, T. Crepaldi, J. L. Crespo, A. Criollo, V. Crippa, M.T. Cruz, A.M. Cuervo, J.M. Cuezva, T.X. Cui, P. R. Cutillas, M.J. Czaja, M.F. Czyzyk-Krzeska, R.K. Dagda, U. Dahmen, C.S. Dai, W. J. Dai, Y. Dai, K.N. Dalby, L.D. Valle, G. Dalmasso, M. D'Amelio, M. Damme, A. Darfeuille-Michaud, C. Dargemont, V.M. Darley-Usmar, S. Dasarathy,

B. Dasgupta, S. Dash, C.R. Dass, H.M. Davey, L.M. Davids, D. Davila, R.J. Davis, T. M. Dawson, V.L. Dawson, P. Daza, J. de Belleroche, P. de Figueiredo, R. de Figueiredo, J. de la Fuente, L. De Martino, A. De Matteis, G.R.Y. De Meyer, A. De Milito, M. De Santi, W. de Souza, V. De Tata, D. De Zio, J. Debnath, R. Dechant, J. P. Decuypere, S. Deegan, B. Dehay, B. Del Bello, D.P. Del Re, R. Delage-Mourroux, L.M.D. Delbridge, L. Deldicque, E. Delorme-Axford, Y.Z. Deng, J. Dengjel, M. Denizot, P. Dent, C.J. Der, V. Deretic, B. Derrien, E. Deutsch, T.P. Devarenne, R. J. Devenish, S. Di Bartolomeo, N. Di Daniele, F. Di Domenico, A. Di Nardo, S. Di Paola, A. Di Pietro, L. Di Renzo, A. DiAntonio, G. Diaz-Araya, I. Diaz-Laviada, M. T. Diaz-Meco, J. Diaz-Nido, C.A. Dickey, R.C. Dickson, M. Diederich, P. Digard, I. Dikic, S.P. Dinesh-Kumar, C. Ding, W.X. Ding, Z.F. Ding, L. Dini, J.H.W. Distler, A. Diwan, M. Djavaheri-Mergny, K. Dmytruk, R.C.J. Dobson, V. Doetsch, K. Dokladny, S. Dokudovskaya, M. Donadelli, X.C. Dong, X.N. Dong, Z. Dong, T. M. Donohue, K.S. Doran, G. D'Orazi, G.W. Dorn, V. Dosenko, S. Dridi, L. Drucker, J. Du, L.L. Du, L.H. Du, A. du Toit, P. Dua, L. Duan, P. Duann, V.K. Dubey, M. R. Duchen, M.A. Duchosal, H. Duez, I. Dugail, V.I. Dumit, M.C. Duncan, E. A. Dunlop, W.A. Dunn, N. Dupont, L. Dupuis, R.V. Duran, T.M. Durcan, S. Duvezin-Caubet, U. Duvvuri, V. Eapen, D. Ebrahimi-Fakhari, A. Echard, L. Eckhart, C. L. Edelstein, A.L. Edinger, L. Eichinger, T. Eisenberg, A. Eisenberg-Lerner, N. T. Eissa, W.S. El-Deiry, V. El-Khoury, Z. Elazar, H. Eldar-Finkelman, C.J.H. Elliott, E. Emanuele, U. Emmenegger, N. Engedal, A.M. Engelbrecht, S. Engelender, J. M. Enserink, R. Erdmann, J. Erenpreisa, R. Eri, J.L. Eriksen, A. Erman, R. Escalante, E.L. Eskelinen, L. Espert, L. Esteban-Martinez, T.J. Evans, M. Fabri, G. Fabrias, C. Fabrizi, A. Facchiano, N.J. Faergeman, A. Faggioni, W.D. Fairlie, C.H. Fan, D. P. Fan, J. Fan, S.Y. Fang, M. Fanto, A. Fanzani, T. Farkas, M. Faure, F.B. Favier, H. Fearnhead, M. Federici, E. Fei, T.C. Felizardo, H. Feng, Y.B. Feng, Y.C. Feng, T. A. Ferguson, A.F. Fernandez, M.G. Fernandez-Barrena, J.C. Fernandez-Checa, A. Fernandez-Lopez, M.E. Fernandez-Zapico, O. Feron, E. Ferraro, C.V. Ferreira-Halder, L. Fesus, R. Feuer, F.C. Fiesel, E.C. Filippi-Chiela, G. Filomeni, G.M. Fimia, J.H. Fingert, S. Finkbeiner, T. Finkel, F. Fiorito, P.B. Fisher, M. Flajolet, F. Flamigni, O. Florey, S. Florio, R.A. Floto, M. Folini, C. Follo, E.A. Fon, F. Fornai, F. Fortunato, A. Fraldi, R. Franco, A. Francois, A. Francois, L.B. Frankel, I.D. C. Fraser, N. Frey, D.G. Freyssenet, C. Frezza, S.L. Friedman, D.E. Frigo, D.X. Fu, J. M. Fuentes, J. Fueyo, Y. Fujitani, Y. Fujiwara, M. Fujiya, M. Fukuda, S. Fulda, C. Fusco, B. Gabryel, M. Gaestel, P. Gailly, M. Gajewska, S. Galadari, G. Galili, I. Galindo, M.F. Galindo, G. Galliciotti, L. Galluzzi, L. Galluzzi, V. Galy, N. Gammoh, S. Gandy, A.K. Ganesan, S. Ganesan, I.G. Ganley, M. Gannage, F. B. Gao, F. Gao, J.X. Gao, L.G. Nannig, E.G. Vescovi, M. Garcia-Macia, C. Garcia-Ruiz, A.D. Garg, P.K. Garg, R. Gargini, N.C. Gassen, D. Gatica, E. Gatti, J. Gavard, E. Gavathiotis, L. Ge, P.F. Ge, S.F. Ge, P.W. Gean, V. Gelmetti, A.A. Genazzani, J. F. Geng, P. Genschik, L. Gerner, J.E. Gestwicki, D.A. Gewirtz, S. Ghavami, E. Ghigo, D. Ghosh, A.M. Giammarioli, F. Giampieri, C. Giampietri, A. Giatromanolaki, D. J. Gibbings, L. Gibellini, S.B. Gibson, V. Ginet, A. Giordano, F. Giorgini, E. Giovannetti, S.E. Girardin, S. Gispert, S. Giuliano, C.L. Gladson, A. Glavic, M. Gleave, N. Godefroy, R.M. Gogal, K. Gokulan, G.H. Goldman, D. Goletti, M. S. Goligorsky, A.V. Gomes, L.C. Gomes, H. Gomez, C. Gomez-Manzano, R. Gomez-Sanchez, D.A.P. Goncalves, E. Goncu, Q.Q. Gong, C. Gongora, C.B. Gonzalez, P. Gonzalez-Alegre, P. Gonzalez-Cabo, R.A. Gonzalez-Polo, I.S. Goping, C. Gorbea, N.V. Gorbunov, D.R. Goring, A.M. Gorman, S.M. Gorski, S. Goruppi, S. Goto-Yamada, C. Gotor, R.A. Gottlieb, I. Gozes, D. Gozuacik, Y. Graba, M. Graef, G. E. Granato, G.D. Grant, S. Grant, G.L. Gravina, D.R. Green, A. Greenhough, M. T. Greenwood, B. Grimaldi, F. Gros, C. Grose, J.F. Groulx, F. Gruber, P. Grumati, T. Grune, J.L. Guan, K.L. Guan, B. Guerra, C. Guillen, K. Gulshan, J. Gunst, C. Y. Guo, L. Guo, M. Guo, W.J. Guo, X.G. Guo, A.A. Gust, A.B. Gustafsson, E. Gutierrez, M.G. Gutierrez, H.S. Gwak, A. Haas, J.E. Haber, S. Hadano, M. Hagedorn, D.R. Hahn, A.J. Halayko, A. Hamacher-Brady, K. Hamada, A. Hamai, A. Hamann, M. Hamasaki, I. Hamer, Q. Hamid, Q. Hamid, F. Han, W.D. Han, J. T. Handa, J.A. Hanover, M. Hansen, M. Harada, L. Harhaji-Trajkovic, J.W. Harper, A.H. Harrath, A.L. Harris, J. Harris, U. Hasler, P. Hasselblatt, K. Hasui, R. G. Hawley, T.S. Hawley, C.C. He, C.Y. He, F.T. He, G. He, R.R. He, X.H. He, Y. W. He, Y.Y. He, J.K. Heath, M.J. Hebert, R.A. Heinzen, G.V. Helgason, M. Hensel, E.P. Henske, C.T. Her, P.K. Herman, A. Hernandez, C. Hernandez, S. Hernandez-Tiedra, C. Hetz, P.R. Hiesinger, K. Higaki, S. Hilfiker, B.G. Hill, J.A. Hill, W.D. Hill, K. Hino, D. Hofius, P. Hofman, G.U. Hoglinger, J. Hohfeld, M.K. Holz, Y.G. Hong, D.A. Hood, J.J.M. Hoozemans, T. Hoppe, C. Hsu, C.Y. Hsu, L.C. Hsu, D. Hu, G. C. Hu, H.M. Hu, H.B. Hu, M.C. Hu, Y.C. Hu, Z.W. Hu, F. Hua, Y. Hua, C.H. Huang, H.L. Huang, K.H. Huang, K.Y. Huang, S.L. Huang, S.Q. Huang, W.P. Huang, Y. R. Huang, Y. Huang, Y.F. Huang, T.B. Huber, P. Huebbe, W.K. Huh, J.J. Hulmi, G. M. Hur, J.H. Hurley, Z. Husak, S.N.A. Hussain, S. Hussain, J.J. Hwang, S. M. Hwang, T.I.S. Hwang, A. Ichihara, Y. Imai, C. Imbriano, M. Inomata, T. Into, V. Iovane, J.L. Iovanna, R.V. Iozzo, N.Y. Ip, J.E. Irazoqui, P. Iribarren, Y. Isaka, A. J. Isakovic, H. Ischiropoulos, J.S. Isenberg, M. Ishaq, H. Ishida, I. Ishii, J.E. Ishmael, C. Isidoro, K.I. Isobe, E. Isono, S. Issazadeh-Navikas, K. Itahana, E. Itakura, A. I. Ivanov, A.K.V. Iyer, J.M. Izquierdo, Y. Izumi, V. Izzo, M. Jaattela, N. Jaber, D. J. Jackson, W.T. Jackson, T.G. Jacob, T.S. Jacques, C. Jagannath, A. Jain, N. R. Jana, B.K. Jang, A. Jani, B. Janji, P.R. Jannig, P.J. Jansson, S. Jean, M. Jendrach, J.H. Jeon, N. Jessen, E.B. Jeung, K.L. Jia, L.J. Jia, H. Jiang, H.C. Jiang, L.W. Jiang, T. Jiang, X.Y. Jiang, X.J. Jiang, X.J. Jiang, Y. Jiang, Y.J. Jiang, A. Jimenez, C. Jin, H.C. Jin, L. Jin, M.Y. Jin, S.K. Jin, U.K. Jinwal, E.K. Jo, T. Johansen, D.E. Johnson, G.V.W. Johnson, J.D. Johnson, E. Jonasch, C. Jones, L.A.B. Joosten, J. Jordan, A. M. Joseph, B. Joseph, A.M. Joubert, D.W. Ju, J.F. Ju, H.F. Juan, K. Juenemann, G. Juhasz, H.S. Jung, J.U. Jung, Y.K. Jung, H. Jungbluth, M.J. Justice, B. Jutten, N. O. Kaakoush, K. Kaarniranta, A. Kaasik, T. Kabuta, B. Kaeffer, K. Kagedal, A. Kahana, S. Kajimura, O. Kakhlon, M. Kalia, D.V. Kalvakolanu, Y. Kamada, K. Kambas, V.O. Kaminskyy, H.H. Kampinga, M. Kandouz, C. Kang, R. Kang, T. C. Kang, T. Kanki, T.D. Kanneganti, H. Kanno, A.G. Kanthasamy, M. Kantorow,

M. Kaparakis-Liaskos, O. Kapuy, V. Karantza, M.R. Karim, P. Karmakar, A. Kaser, S. Kaushik, T. Kawula, A.M. Kaynar, P.Y. Ke, Z.J. Ke, J.H. Kehrl, K.E. Keller, J. K. Kemper, A.K. Kenworthy, O. Kepp, A. Kern, S. Kesari, D. Kessel, R. Ketteler, I. D. Kettelhut, B. Khambu, M.M. Khan, V.K.M. Khandelwal, S. Khare, J.G. Kiang, A. A. Kiger, A. Kihara, A.L. Kim, C.H. Kim, D.R. Kim, D.H. Kim, E.K. Kim, H.Y. Kim, H. R. Kim, J.S. Kim, J.H. Kim, J.C. Kim, J.H. Kim, K.W. Kim, M.D. Kim, M.M. Kim, P. K. Kim, S.W. Kim, S.Y. Kim, Y.S. Kim, Y. Kim, A. Kimchi, A.C. Kimmelman, T. Kimura, J.S. King, K. Kirkegaard, V. Kirkin, L.A. Kirshenbaum, S. Kishi, Y. Kitajima, K. Kitamoto, Y. Kitaoka, K. Kitazato, R.A. Kley, W.T. Klimecki, M. Klinkenberg, J. Klucken, H. Knaevelsrud, E. Knecht, L. Knuppertz, J.L. Ko, S. Kobayashi, J.C. Koch, C. Koechlin-Ramonatxo, U. Koenig, Y.H. Koh, K. Kohler, S. D. Kohlwein, M. Koike, M. Komatsu, E. Kominami, D.X. Kong, H.J. Kong, E. G. Konstantakou, B.T. Kopp, T. Korcsmaros, L. Korhonen, V.I. Korolchuk, N. V. Koshkina, Y.J. Kou, M.I. Koukourakis, C. Koumenis, A.L. Kovacs, T. Kovacs, W. J. Kovacs, D. Koya, C. Kraft, D. Krainc, H. Kramer, T. Kravic-Stevovic, W. Krek, C. Kretz-Remy, R. Krick, M. Krishnamurthy, J. Kriston-Vizi, G. Kroemer, M. C. Kruer, R. Kruger, N.T. Ktistakis, K. Kuchitsu, C. Kuhn, A.P. Kumar, A. Kumar, A. Kumar, D. Kumar, D. Kumar, R. Kumar, S. Kumar, M. Kundu, H.J. Kung, A. Kuno, S.H. Kuo, J. Kuret, T. Kurz, T. Kwok, T.K. Kwon, Y.T. Kwon, I. Kyrmizi, A. R. La Spada, F. Lafont, T. Lahm, A. Lakkaraju, T. Lam, T. Lamark, S. Lancel, T. H. Landowski, D.J.R. Lane, J.D. Lane, C. Lanzi, P. Lapaquette, L.R. Lapierre, J. Laporte, J. Laukkarinen, G.W. Laurie, S. Lavandero, L. Lavie, M.J. LaVoie, B.Y. K. Law, H.K.W. Law, K.B. Law, R. Layfield, P.A. Lazo, L. Le Cam, K.G. Le Roch, H. Le Stunff, V. Leardkamolkarn, M. Lecuit, B.H. Lee, C.H. Lee, E.F. Lee, G.M. Lee, H.J. Lee, H. Lee, J.K. Lee, J. Lee, J.H. Lee, J.H. Lee, M. Lee, M.S. Lee, P.J. Lee, S. W. Lee, S.J. Lee, S.J. Lee, S.Y. Lee, S.H. Lee, S.S. Lee, S.J. Lee, S. Lee, Y.R. Lee, Y. J. Lee, Y.H. Lee, C. Leeuwenburgh, S. Lefort, R. Legouis, J.Z. Lei, Q.Y. Lei, D. A. Leib, G. Leibowitz, I. Lekli, S.D. Lemaire, J.J. Lemasters, M.K. Lemberg, A. Lemoine, S.L. Leng, G. Lenz, P. Lenzi, L.O. Lerman, D.L. Barbato, J.I.J. Leu, H. Y. Leung, B. Levine, P.A. Lewis, F. Lezoualc'h, C. Li, F.Q. Li, F.J. Li, J. Li, K. Li, L. Li, M. Li, M. Li, Q. Li, R. Li, S. Li, W. Li, W. Li, X.T. Li, Y.M. Li, J.Q. Lian, C.Y. Liang, Q. R. Liang, Y.L. Liao, J. Liberal, P.P. Liberski, P. Lie, A.P. Lieberman, H.J. Lim, K. L. Lim, K. Lim, R.T. Lima, C.S. Lin, C.F. Lin, F. Lin, F.M. Lin, F.C. Lin, K. Lin, K. H. Lin, P.H. Lin, T.W. Lin, W.W. Lin, Y.S. Lin, Y. Lin, R. Linden, D. Lindholm, L. M. Lindqvist, P. Lingor, A. Linkermann, L.A. Liotta, M.M. Lipinski, V.A. Lira, M. P. Lisanti, P.B. Liton, B. Liu, C. Liu, C.F. Liu, F. Liu, H.J. Liu, J.X. Liu, J.J. Liu, J. L. Liu, K. Liu, L.Y. Liu, L. Liu, Q.T. Liu, R.Y. Liu, S.M. Liu, S.W. Liu, W. Liu, X.D. Liu, X.G. Liu, X.H. Liu, X.F. Liu, X. Liu, X.Q. Liu, Y. Liu, Y.L. Liu, Z.X. Liu, Z. Liu, J. P. Liuzzi, G. Lizard, M. Ljujic, I.J. Lodhi, S.E. Logue, B.L. Lokeshwar, Y.C. Long, S. Lonial, B. Loos, C. Lopez-Otin, C. Lopez-Vicario, M. Lorente, P.L. Lorenzi, P. Lorincz, M. Los, M.T. Lotze, P.E. Lovat, B.F. Lu, B. Lu, J. Lu, Q. Lu, S.M. Lu, S. Y. Lu, Y.Y. Lu, F. Luciano, S. Luckhart, J.M. Lucocq, P. Ludovico, A. Lugea, N. W. Lukacs, J.J. Lum, A.H. Lund, H.L. Luo, J. Luo, S.Q. Luo, C. Luparello, T. Lyons, J.J. Ma, Y. Ma, Y. Ma, Z.Y. Ma, J. Machado, G.M. Machado-Santelli, F. Macian, G. C. MacIntosh, J.P. MacKeigan, K.F. Macleod, J.D. MacMicking, L.A. MacMillan-Crow, F. Madeo, M. Madesh, J. Madrigal-Matute, A. Maeda, T. Maeda, G. Maegawa, E. Maellaro, H. Maes, M. Magarinos, K. Maiese, T.K. Maiti, L. Maiuri, M.C. Maiuri, C.G. Maki, R. Malli, W. Malorni, A. Maloyan, F. Mami-Chouaib, N. Man, J.D. Mancias, E.M. Mandelkow, M.A. Mandell, A.A. Manfredi, S.N. Manie, C. Manzoni, K. Mao, Z.X. Mao, Z.W. Mao, P. Marambaud, A.M. Marconi, Z. Marelja, G. Marfe, M. Margeta, et al., Guidelines for the use and interpretation of assays for monitoring autophagy (3rd edition), Autophagy 12 (2016) 1–222, https://doi.org/10.1080/15548627.2015.1100356.

[72] M.R. Block, C. Badowski, A. Millon-Fremillon, D. Bouvard, A.P. Bouin, E. Faurobert, D. Gerber-Scokaert, E. Planus, C. Albiges-Rizo, Podosome-type adhesions and focal adhesions, so alike yet so different, Eur. J. Cell Biol. 87 (2008) 491–506, https://doi.org/10.1016/j.ejcb.2008.02.012.

[73] K. Legerstee, B. Geverts, J.A. Slotman, A.B. Houtsmuller, Dynamics and distribution of paxillin, vinculin, zyxin and VASP depend on focal adhesion location and orientation, Sci. Rep. 9 (2019) 18, https://doi.org/10.1038/s41598-019-46905-2.

[74] A. Van den Abbeele, S. De Clercq, A. De Ganck, V. De Corte, B. Van Loo, S.H. Soror, V. Srinivasan, J. Steyaert, J. Vandekerckhove, J. Gettemans, A llama-derived gelsolin single-domain antibody blocks gelsolin-G-actin interaction, Cell. Mol. Life Sci. 67 (2010) 1519–1535, https://doi.org/10.1007/s00018-010-0266-1.

[75] D. Manna, A. Albanese, W.S. Park, W. Cho, Mechanistic basis of differential cellular responses of phosphatidylinositol 3,4-bisphosphate- and phosphatidylinositol 3,4,5-trisphosphate-binding pleckstrin homology domains, J. Biol. Chem. 282 (2007) 32093–32105, https://doi.org/10.1074/jbc.M703517200.

[76] E.J. Dickson, B. Hille, Understanding phosphoinositides: rare, dynamic, and essential membrane phospholipids, Biochem. J. 476 (2019) 1–23, https://doi.org/10.1042/bcj20180022.

[77] K. Du, P.N. Tsichlis, Regulation of the Akt kinase by interacting proteins, Oncogene 24 (2005) 7401–7409, https://doi.org/10.1038/sj.onc.1209099.

[78] Y. Bai, J.Y. Li, J. Li, Y.H. Liu, B. Zhang, MiR-615 inhibited cell proliferation and cell cycle of human breast cancer cells by suppressing of AKT2 expression, Int. J. Clin. Exp. Med. 8 (2015) 3801–3808.

[79] W. Ouyang, J.X. Li, Q. Ma, C.S. Huang, Essential roles of PI-3K/Akt/IKK beta/NF kappa B pathway in cyclin D1 induction by arsenite in JB6 Cl41 cells, Carcinogenesis 27 (2006) 864–873, https://doi.org/10.1093/carcin/bgi321.

[80] X.B. Deng, J. Hu, D.Z. Ewton, E. Friedman, Mirk/dyrk1B kinase is upregulated following inhibition of mTOR, Carcinogenesis 35 (2014) 1968–1976, https://doi.org/10.1093/carcin/bgu058.

[81] J.S. Brown, U. Banerji, Maximising the potential of MKT inhibitors as anti-cancer treatments, Pharmacol. Ther. 172 (2017) 101–115, https://doi.org/10.1016/j.pharmthera.2016.12.001.

[82] A. Carracedo, P.P. Pandolfi, The PTEN-PI3K pathway: of feedbacks and cross-talks, Oncogene 27 (2008) 5527–5541, https://doi.org/10.1038/onc.2008.247.

[83] H.M. Xu, F. Hu, The role of autophagy and mitophagy in cancers, Arch. Physiol. Biochem. (2019) 9, https://doi.org/10.1080/13813455.2019.1675714.

[84] J. Pignatelli, S.E. LaLonde, D.P. LaLonde, D. Clarke, C.E. Turner, Actopaxin (alpha-Parvin) phosphorylation is required for matrix degradation and Cancer cell invasion, J. Biol. Chem. 287 (2012) 37309–37320, https://doi.org/10.1074/jbc.M112.385229.

[85] J.L. Zhou, Y.J. Zeng, L. Cui, X.C. Chen, S. Stauffer, Z. Wang, F. Yu, S.M. Lele, G. A. Talmon, A.R. Black, Y.H. Chen, J.X. Dong, Zyxin promotes colon cancer tumorigenesis in a mitotic phosphorylation-dependent manner and through CDK8-mediated YAP activation, Proc. Natl. Acad. Sci. U. S. A. 115 (2018) E6760–E6769, https://doi.org/10.1073/pnas.1800621115.

[86] A.D.G. Lawson, Antibody-enabled small-molecule drug discovery, Nat. Rev. Drug Discov. 11 (2012) 519–525, https://doi.org/10.1038/nrd3756.

[87] J.B. Dong, A.A. Thompson, Y.F. Fan, J.L. Lou, F. Conrad, M.F. Ho, M. Pires-Alves, B.A. Wilson, R.C. Stevens, J.D. Marks, A single-domain llama antibody potently inhibits the enzymatic activity of botulinum neurotoxin by binding to the non-catalytic alpha-exosite binding region, J. Mol. Biol. 397 (2010) 1106–1118, https://doi.org/10.1016/j.jmb.2010.01.070.